

Minimum Velocity Dispersion in Stable Stellar Disks. Numerical Simulations

*A. V. Khoperskov*¹, *A. V. Zasov*², *N. V. Tyurina*³

¹ Sternberg Astronomical Institute, Universitetskii pr. 13, Moscow, 119992 Russia;
Volgograd State University;
khopersk@sai.msu.ru

² Sternberg Astronomical Institute, Universitetskii pr. 13, Moscow, 119992 Russia;
zasov@sai.msu.ru

³ Sternberg Astronomical Institute, Universitetskii pr. 13, Moscow, 119992 Russia;
tiurina@sai.msu.ru

Abstract

We used N -body dynamical simulations to analyze the conditions for the gravitational stability of a three-dimensional stellar disk in the gravitational field of two rigid spherical components — a bulge and a halo, whose central concentrations and relative masses vary over wide ranges. The number of point masses N in the simulations varied from 40 to 500 thousands and the evolution of the simulated models is followed over 10–20 rotation periods of the outer edge of the disk. The initially unstable disks are heated and, as a rule, reach a quasi-stationary equilibrium with a steady-state radial-velocity dispersion c_r over five to eight periods of rotation. The radial behavior of the Toomre stability parameter $Q_T(r)$ for the final state of the disk is estimated. Numerical models are used to analyze the dependence of the gravitational stability of the disk on the relative masses of the spherical components, disk thickness, degree of differential rotation, and initial state of the disk. Formal application of existing analytical local criteria for marginal stability of the disk can lead to errors in c_r of more than a factor of 1.5. It is suggested that the approximate constancy of $Q_T \simeq 1.2 \div 1.5$ for $r \simeq (1 \div 2) \times L$ (where L is the radial scale of a disk surface density), valid for a wide range of models, can be used to estimate upper limits for the disc mass and density based on the observed distributions of the rotational velocity of the gaseous component and of the stellar velocity dispersion.

1 INTRODUCTION

Galactic disks, which consist mostly of old stars, can be considered as collisionless systems in quasi-stationary equilibrium with very slow evolution. This state is characterized by certain radial dependences of the stellar velocity dispersions (c_r, c_φ, c_z) that ensure stability of the disk. Knowledge of the stability conditions makes it possible to develop self-consistent models for the disks of real galaxies for which both the rotational velocities and stellar velocity dispersions have been measured at various galactocentric distances.

The problem of determining the minimum stellar velocity dispersion sufficient to ensure stability of the disk against arbitrary perturbations is especially important if, as many authors have suggested (see, e.g., [1–7]), real galaxies may be in a state of threshold (marginal) stability. This approach enables the local density or integrated mass of the disk to be estimated from the observed velocity dispersion. In the general case, the old stellar population of a galactic disk can have an excess velocity dispersion in the presence of other factors that heat the disk, which are not directly related to the gravitational instability. However, even in this case, the conditions for marginal stability provide valuable information by yielding an upper limit for the mass of the disk that enables it to be stable.

Fridman and Polyachenko [8, 9] carried out a detailed theoretical analysis of the stability of thin rotating disks against different kinds of perturbations (including bending modes). Together with certain advantages over numerical simulations (the mathematical rigorousness of the solutions in the framework of the problem formulated), the analytical approach to the dynamics of perturbations in a gravitating disk and the conditions for

stability has the drawback that it can be implemented only for very simple models and can yield only coarse estimates for the parameters of the disk component when applied to real objects. Let us consider these simplifications in more detail.

First and foremost, the simple analytical models of collisionless disks that are used in stability analyses usually assume that the disk thickness is small; they actually consider an infinitely thin layer. Despite the smallness of the ratios h_z/r and h_z/L over most of the stellar disk (here, r is the radial coordinate, h_z is the vertical scale height, and L is the radial scale length of the disk), this condition may not be sufficient to justify neglect of vertical motions (see Gor’kavyi and Fridman [10, Appendix II¹] for a detailed discussion of this issue; in the general case, the dynamics equations for astrophysical disks cannot be adequately treated in a two-dimensional formulation).

Analytical studies of the dynamics of small perturbations in a stellar disk usually assume that the disk parameters have small radial gradients (see, e.g., [1, 11, 12]). Attempts to allow for gradients have thus far been made only in terms of WKB approximations (see, e.g., [2, 13–15]). This means that the characteristic perturbation wavelength is short compared to the local scale lengths for variations of the circular velocity $V(r)$, stellar radial-velocity dispersion $c_r(r)$, and surface

density $\sigma(r)$. In many cases, these conditions are barely satisfied or even not satisfied. Taking into account differential rotation may pose the most difficult problem. Allowance for weakly differential rotation is possible for small nonradial perturbations [13, 16]. However, nonaxisymmetric

¹Written in coauthorship with O.V. Khoruzhiĭ.

(in the limiting case, spoke-like) perturbations are more unstable. Their stabilization under the same conditions requires significantly stronger disk heating, i.e., a higher stellar velocity dispersion [17], and these very perturbations apparently increase the stellar velocity dispersion at the nonlinear stage in the case of initially cool systems.

Analytical studies of the gravitational stability of disks usually apply the epicyclic approximation $c_r \ll V$, which is valid at the peripheries of most galaxies, where $c_r/V \simeq 0.1 \div 0.3$, but breaks down near their centers, where $c_r \gtrsim V$.

Another important limitation of analytical approaches is that the criteria derived are local, whereas a number of studies suggest that the disk stability conditions have a global nature [18, 19]. This means that the equilibrium parameters, e.g., at the center, while leaving their values at the disk periphery unchanged, may affect the conditions for gravitational stability throughout the disk. In contrast to a local approach based on the analysis of dispersion equations, global analyses aim to determine the eigenfrequency for the entire disk by solving a boundary-value problem, which determines the influence of the conditions in one part of the system on the dispersion properties of the perturbations throughout the disk. Therefore, in a rigorous approach, the disk must be considered as a whole. However, global analyses have been performed only for certain specific power-law distributions [18–20]. For example, Bertin *et al.* [21] considered global modes in galactic disks as possible mechanisms for maintaining long-lived spiral density waves.

Numerical simulations of collisionless systems are more flexible in terms of the choice of model. They make it possible to go beyond simple two-dimensional models and directly follow the development of perturbations in a disk that is initially in equilibrium. However, this approach has drawbacks of its own. The most serious problems of N -body simulations include (1) certain mathematical simplifications that are inevitable when a disk is modeled as a system of N gravitating bodies, where N is incomparably smaller than the number of stars in real galaxies, and (2) the dependence of the final state of the system (after it reaches quasi-equilibrium) on the initial parameters, which are poorly known for real galaxies. When comparing simulation results with real galaxies, it can also be difficult to allow for the dissipative galactic medium (gas), in which the sound speed is much lower than the stellar velocity dispersion. We consider these problems in more detail below.

The principal goal of this study is to determine for galaxies with various mass distributions the minimum local disk velocity dispersions that enable their three-dimensional disks, which are initially in a weakly unstable equilibrium, to reach a quasi-stationary state. Sections 2 and 3 give a concise review of previous results of analytical and numerical approaches to estimating the stellar velocity dispersions required to ensure the stability of collisionless disks. Section 4 describes the principles underlying the construction of the dynamical models and the determination of the stability threshold used in this paper. Section 5 considers various three-dimensional models of galaxies, and the last section presents and discusses the main results.

2 ANALYTICAL STABILITY CRITERIA

Several criteria for gravitational instability derived analytically using various models have been published. Let us review those we consider to be most important.

(a) The Toomre Criterion

In order for an infinitely thin, uniform, rigidly rotating stellar disk to be gravitationally stable against axisymmetric perturbations, it must satisfy the following condition derived by Toomre [1]:

$$c_r \geq c_T = \frac{3.36G\sigma}{\varkappa}, \quad Q_T = \frac{c_r}{c_T} \geq 1, \quad (1)$$

where $\varkappa = 2\Omega\sqrt{1 + rd\Omega/2\Omega dr}$ is the epicyclic frequency and σ is the surface density. Condition (1) assumes that the epicyclic approximation is valid, i.e., that the difference between the velocity $V(r)$ and the circular velocity $V_c(r)$ can be neglected. Although this relation was derived in a local analysis, the study of Evans and Read [19] of the eigenmodes for self-similar disks in a corresponding approximation overall supports its validity. Miller [22] compared the theoretical increments derived for a Toomre model with the results of simulations of axisymmetric modes in which all other perturbations were artificially suppressed. Experimental gradients were shown to be consistent with the theoretical results.

(b) Allowance for Finite Disk Thickness

Finite thickness is a stabilizing factor for gravitational instability in the plane of the disk [9, 12]. The generalization of the Toomre stability criterion (1) for the case of a disk of finite thickness obtained by Morozov [13, 14, 16] has the form

$$Q_T^{(1)} = \frac{1}{1 + 0.974\Delta\varkappa/c_r} < 1, \quad (2)$$

where Δ is the half-thickness of the isothermal self-gravitating disk. However, this condition proved to be far from sufficient to ensure the stability of real systems. This became clear from the first numerical simulations performed in the 1970s, which showed that $c_r \simeq (1.5 \div 5) \times c_T$ at the periphery of a stationary, collisionless disk [23–30].

(c) Simplified Allowance for Nonaxisymmetric Perturbations

The stronger instability of spiral waves compared to axisymmetric modes is one of the factors that makes the Toomre criterion inadequate. Polyachenko and Shukhman [31], Kalnajs [32], and Polyachenko and Fridman [9] were the first to show that nonaxisymmetric modes are the dominant instabilities in a gravitationally unstable disk. As pointed out by Polyachenko and Fridman [9], the azimuthal-velocity dispersion c_φ is smaller than c_r (except for the innermost regions). Therefore, the relation

$$c_\varphi = c_r \frac{\varkappa}{2\Omega}, \quad (3)$$

implies that, in order for an azimuthally cooler disk to be stabilized, it must be heated more strongly, so that, in view of (3), the condition (1) can be rewritten in the form

$$Q_T^{(2)} \geq S, \quad \text{where } S = \frac{2\Omega}{\varkappa}. \quad (4)$$

The parameter S characterizes the degree of differential rotation of the disk. In most cases, we can assume that $1 \leq S \leq 2$, based on the observed shapes of galactic rotation curves. This form of the stability condition is discussed in [13–16].

Thus, the azimuthal velocity dispersion determines the elasticity of the medium against strongly nonaxisymmetric perturbations, so that the suppression of gravitational instability requires stronger heating of the disk by a factor of $2\Omega/\varkappa$.

Criterion (4) can be considered to be the Toomre criterion with a simplified allowance for nonaxisymmetric perturbations.

(d) The Morozov Criterion

Morozov [13], Morozov and Khoperskov [14], and Morozov [16] analyzed the dynamics of weakly nonradial perturbations in a nonuniform disk in a WKB approximation. The resulting stability criterion takes into account many factors (radial nonuniformity of the surface density σ and radial-velocity dispersion c_r , the disk thickness, and differential rotation):

$$Q_T^{(M)} = c^{(M)}/c_T, \quad c^{(M)} = S D c_T \left\{ 1 + 1.07 \cdot \left| 1.87 S \frac{c_T}{\varkappa} \left(\frac{d\sigma}{\sigma dr} + \frac{dS}{S dr} - 1.09 \frac{dc^{(M)}}{c^{(M)} dr} \right) \right|^{2/3} \right\}, \quad (5)$$

where $S = 2\Omega/\varkappa$ and $D = (1 + 0.974\varkappa\Delta/(S^2c_T))^{-1}$.

In the general case, determining $c^{(M)}$ from (5) amounts to integrating a reduced differential equation [33]. The main drawback of this criterion is that it was derived in the context of the dynamics of tightly wound spiral waves ($m/r \ll k_r$, where k_r is the radial wavenumber) and then formally applied to spokelike perturbations.

If the scale length $L_c \equiv (d \ln c^{(M)}/dr)^{-1}$ is fixed, the differential equation (5) reduces to a simple algebraic relation [13, 14, 16]. For typical rotation-curve shapes, we have $D \simeq 0.6 \div 0.8$. Introducing the factor D also makes it possible to formally allow for the disk thickness in criteria (3) and (6).

(e) The Polyachenko–Polyachenko–Strel’nikov Criterion

Unlike the criteria discussed above, the analysis of Polyachenko *et al.* [17] focused on extremely nonaxisymmetric perturbations in a thin disk. Under the assumptions made, the rotation curve is the sole factor determining the stability boundary, since this boundary depends only on the parameter $n \equiv -rd\Omega/(\Omega dr)$. Figure 1 in [17] shows the dependence of the dimensionless velocity dispersion at the stability boundary on the parameter $\alpha = 2/n$. We will use the approximating function

$$Q_T^{(P)} = \frac{c^{(P)}}{c_T} = 1.88 \sqrt{1.1 + \frac{8}{\exp(\alpha - 1/4) - 1}}, \quad (6)$$

where $Q_T^{(P)}$ is the minimum Toomre parameter for a stable disk.

This approximation has sufficient accuracy for our needs when $1.2 < \alpha^2$. The criterion of Polyachenko *et al.* [17] depends on a single parameter, since the form of the rotation curve fully determines the stability boundary. In particular, it follows that $Q_T^{(P)} \simeq 3$ in the region with constant rotational velocity ($n = 1$).

(f) Allowance for the Gaseous Subsystem in a Stability Analysis for Stellar Disks

The presence of a cooler component also contributes to destabilization of the stellar disk. A number of authors [34–38] have analyzed this problem in detail as applied to radial perturbations.

Ortega *et al.* [38] considered a more general problem: they analyzed how the inhomogeneous composition of a thin disk influences the stability of the disk against small radial perturbations when the disk consists of particles having a mass spectrum such that more massive particles have lower velocity dispersions.

The problem is simplified if the mass of the “cool” component is relatively small. Assuming the gas surface density σ_{gas} to be usually much lower than the surface density of the stellar disk σ_{star} and $c_s \ll c_r$ (where c_s is the adiabatic sound speed in the gas), one can write for the velocity dispersion of a stellar disk containing gas at the stability boundary [37]

$$\frac{c_r^{\text{crit}}}{c_T} = 1 + \frac{\sigma_{\text{gas}}}{\sigma_{\text{gas}} + \sigma_{\text{star}}} \frac{1 - (c_s/c_T)^2}{1 + (c_s/c_T)^2}. \quad (7)$$

For example, for the parameters of the solar neighborhood in the Galaxy, it follows from (7) that the gaseous subsystem, which contributes about 20% of the disk surface density, increases the minimum stellar-velocity dispersion sufficient for stabilizing radial perturbations by $\leq 10\%$.

Finally, we note that attempts have also been made to determine the parameters of the disk subsystem using other approaches based on the possible existence of various structures in the disk (spiral density waves or a bar) rather than on local stability conditions, assuming certain mechanisms that form and sustain these structures. However, the analysis of these approaches is beyond the scope of this paper.

3 ANALYSIS OF GRAVITATIONAL STABILITY IN NUMERICAL SIMULATIONS

Numerical simulations describing the dynamical evolution of disks can be used to analyze disk instabilities for given initial conditions allowing for nonuniform distributions of the mass and angular velocity. Such simulations naturally take into account the formation of appreciably nonlinear and nonaxisymmetric structures such as bars or transient spirals. The main problem with this approach is that the results depend on the initial conditions, since the evolution of a disk starting from a strongly unstable state can proceed very differently from the evolution of a disk starting in a subcritical state. In addition, the disk can suffer from slow secular instabilities that are difficult to take into account in numerical simulations.

N -body evolutionary models are usually aimed at studying the development of instability or — which is of the most interest for us — at analyzing the states of a system after many disk rotations. Of the large number of published studies of this type, we will mention those that are, in our view, most important in the context of establishing the conditions for stability of a disk.

Carlberg and Sellwood [39, 40] analyzed the influence of small, nonstationary perturbations of the potential on the evolution of the velocity-distribution function. In particular, they analyzed scattering by nonstationary spiral waves; the resulting growth of the stellar-velocity dispersion agrees well with the results of numerical simulations.

The critical velocity dispersion for stellar disks (the parameter Q_T) has been computed many times based on the results of N -body dynamical simulations (see, e.g., [7, 24, 28, 33, 40–46]). None

of the simulations yielded a stable disk with $Q_T < 1$. As a rule, $Q_T(r)$ increases with distance from the center of a galaxy. This pattern appears both in simulations of three-dimensional disks [5, 46–48] and in some theoretical analyses [49].

The work of Athanassoula and Sellwood [34] can be considered to be classic. They concluded that a two-dimensional disk is always stable if its Toomre parameter exceeds $Q_T \gtrsim 2.2 \div 2.4$. However, this conclusion did not take into account vertical motions. Since three-dimensional disks are gravitationally more stable, two-dimensional models underestimate the mass of a marginally stable disk. In addition, Athanassoula and Sellwood [34] used a radially averaged Q_T and simulated a specific density distribution based on a Toomre–Kuz'min model. It is therefore not clear whether their results are applicable for real three-dimensional disks.

4 NUMERICAL MODELS: SPECIFYING INITIAL CONDITIONS

The dynamical models used in this paper are based on numerical integration of the equations of motion for N gravitationally interacting particles taking into account the external field produced by the steady-state mass distribution in the bulge and halo.

For the halo, we adopted the commonly used spatial distribution of the volume density in the form

$$\varrho_h(r) = \frac{\varrho_{h0}}{(1 + \xi^2/a^2)^k}, \quad (8)$$

where $\xi = \sqrt{r^2 + z^2}$ is the radial coordinate. Choosing $k = 1$ yields a flat rotation curve in the halo-dominated region. The relative central density of the spherical component increases with k , imitating the influence of the bulge. Because the bulge enters our model as a separate spherical component, we restrict our analysis to a halo model with $k = 1$.

The following set of equations describes the dynamics of the N gravitating bodies:

$$\frac{d^2 \vec{r}_i}{dt^2} = \sum_j^N \vec{f}_{ij} + \vec{F}_s \quad (i = 1, \dots, N), \quad (9)$$

Here, the radius vector $\vec{r}_i(t)$ determines the position of the i th particle, \vec{f}_{ij} is the force of interaction between the i th and j th particles, and the force $\vec{F}_s = \vec{F}_b + \vec{F}_h$ is due to the bulge/halo spheroidal subsystem. The halo mass distribution (8) with a central density of $\varrho_{h0} = M_h / \{4\pi a^3 [R/a - \tan(R/a)]\}$ yields for the force

$$\vec{F}_h(\vec{r}) = -\frac{4\pi G a^3 \varrho_{h0}}{\xi^2} \left\{ \frac{\xi}{a} - \arctg\left(\frac{\xi}{a}\right) \right\} \frac{\vec{r}}{\xi} \quad (10)$$

which is determined by the spatial scale lengths a and mass M_h inside the sphere $\xi = |\mathbf{r}| < R$. We adopt a King model for the density distribution in the spherical bulge:

$$\varrho_b = \begin{cases} \varrho_{b0} / [1 + (\xi/b)^2]^{3/2} & , \quad \xi < (r_b)_{\max} \\ 0 & , \quad \xi > (r_b)_{\max} \end{cases} \quad (11)$$

where

$$M_b = 4\pi b^3 \varrho_{b0} \left\{ \ln \left[(r_b)_{\max}/b + \sqrt{1 + ((r_b)_{\max}/b)^2} \right] - \frac{(r_b)_{\max}/b}{\sqrt{1 + ((r_b)_{\max}/b)^2}} \right\} \quad (12)$$

is the mass of the bulge. We have for the gravitational force inside $\xi \leq (r_b)_{\max}$

$$\vec{F}_b = -\frac{4\pi G b^3 \varrho_{b0}}{\xi^2} \left\{ \ln \left(\frac{\xi}{b} + \sqrt{1 + \frac{\xi^2}{b^2}} \right) - \frac{\xi/b}{\sqrt{1 + \xi^2/b^2}} \right\} \frac{\vec{r}}{\xi}. \quad (13)$$

It is obvious that $\mathbf{F}_b = -GM_b \mathbf{r}/\xi^3$ in the domain $r > (r_b)_{\max}$.

The dynamical model must adequately describe the Newtonian interactions between stars and ensure that the system is collisionless. This is achieved by modifying the gravitational force at small distances by introducing a potential-cutoff radius r_c for any pair of interacting particles i and j . The optimum choice of cutoff radius and number of particles has been widely discussed in the literature (see, e.g., [50–53] and references therein).

Here, we use a Plummer model for the potential:

$$\Phi_{ij} = -G \frac{m_i m_j}{\sqrt{r_{ij}^2 + r_c^2}}, \quad (14)$$

where r_{ij} is the distance between particles and r_c is the cutoff radius. For a fixed number of particles N , it is always possible to choose a cutoff radius r_c that ensures that the model is collisionless. However, the number of particles must be sufficiently large to minimize the error introduced by the modification of the particle-interaction potential at small distances.

We characterize the disk surface density by the scale length L , which determines the exponential law $\sigma(r) = \sigma_0 \exp(-r/L)$. We assumed that the disk surface density is zero in the region $r \geq 5L$ at the beginning of the simulations. We used a system of units in which $G = 1$, $R = 4L = 1$, and the mass of the disk is $M_{\text{d}} = 1$. We normalized the mass of the halo M_h inside the radius $\xi \leq 4L$ to the mass of the disk, $\mu \equiv M_h/M_{\text{d}}$. In this system of units, one period of rotation of the outer edge of the disk lies in the range $t \sim 3 \div 4$ for $\mu = 1 \div 4$.

Let us now describe the procedure for specifying the initial density distribution along z axis and the residual velocities of the equilibrium disk.

The vertical structure of the disk is determined by the equations [54]

$$\frac{1}{r} \frac{\partial}{\partial r} \left(r \frac{\partial \Phi}{\partial r} \right) + \frac{\partial^2 \Phi}{\partial z^2} = 4\pi G (\varrho + \varrho_s), \quad c_z^2 \frac{\partial \varrho}{\partial z} = -\frac{\partial \Phi}{\partial z} \varrho, \quad (15)$$

where ϱ and ϱ_s are the spatial density in the disk and spheroidal subsystems, respectively, and c_z is the vertical-velocity dispersion, which is assumed to remain constant with z at $t = 0$. Eliminating the potential Φ from (15) and introducing the circular velocity

$$V_c(r) \equiv \sqrt{r \left(\frac{\partial \Phi}{\partial r} \right) \Big|_{z=0}}, \quad (16)$$

we can transform the set of partial differential equations to an approximate equation for the disk volume density $\varrho(z)$ in the form of an ordinary differential equation [54]:

$$\varrho \frac{d}{dz} \left(c_z^2 \frac{d\varrho}{dz} \right) - c_z^2 \left(\frac{d\varrho}{dz} \right)^2 + 4\pi G \varrho^2 (\varrho + E + \varrho_s(z)) = 0, \quad E = -\frac{1}{4\pi G r} \frac{dV_c^2}{dr}. \quad (17)$$

Together with the conditions $\varrho(z=0) = \varrho_0$, $d\varrho(0)/dz = 0$, and $\int_{-\infty}^{\infty} \varrho(z; r) dz = \sigma(r)$, this equation determines the vertical structure of the disk at the radius r for a given surface-density distribution σ . The E term can produce a large error in the estimated density at the disk center, and, in practice, it is assumed that $E(r \rightarrow 0) \rightarrow 0$. To determine ϱ_0 and $\varrho(z)$ for specified $\varrho_s(z, r)$, $c_z(z, r)$, and $\sigma(r)$, we construct the function $F(\varrho_0) = 2 \int_0^{\infty} \varrho(z) dz - \sigma$. We solve the equation $F(\varrho_0) = 0$ iteratively jointly with numerical integration (17). After determining the density distribution in z , the particles are arranged along the vertical axis on a grid $z_k = k\Delta z$ ($k = -K, \dots, K$). The k th cell contains particles in proportion to σ_k/σ , where $\sigma_k = \int_{z_{k-1}}^{z_k} \varrho(z) dz$.

Equation (17) is approximate, since it was derived neglecting the dependence of the potential on the vertical coordinate in the first term in (15). Strictly speaking, a disk constructed in this way is not in equilibrium. However, we are interested in initial, unstable states that evolve to new stationary states of the disk. Therefore, the lack of an exact equilibrium in the vertical direction plays the role of a small additional initial perturbation.

The initial velocity distribution is a Schwarzschild function and has the form of an anisotropic Maxwellian distribution:

$$f(u, v, w) = A \exp \left\{ -\frac{u^2}{2c_r^2} - \frac{(v - r\Omega)^2}{2c_\varphi^2} - \frac{w^2}{2c_z^2} \right\},$$

where $\{u, v, w\}$ are the velocity components of the particles in cylindrical coordinates.

To obtain the model with the minimum velocity dispersion in the final, stable disk state, we chose a subcritical disk state whose dynamical evolution ensured both the preservation of an exponential surface-density profile and stability against initial perturbations in the plane of the disk and against bending perturbations (responsible for the increase in the vertical velocity dispersion) at the end of the computations.

In practice, the initial radial-velocity dispersions c_r in models with low-mass bulges corresponded to Toomre parameters $Q_T \simeq 0.8 \div 1.1$ and $Q_T \simeq 1.2 \div 2.2$ in the central region ($r \lesssim 2L$) and at edge of the disk, respectively. In the case of massive bulges, the models started from higher central values of Q_T . The initial vertical-velocity dispersion was set c_z proportional to c_r . We considered two types of models with different initial disk thicknesses: “thin” disks unstable in the z direction², which had central $(c_z/c_r)_0$ values $(c_z/c_r)_0 = (0.4 \div 0.5)$ at $t = 0$, and “thick” disks with $(c_z/c_r)_0 = (0.6 \div 0.8)$, which are close to the stability limit against bending perturbations. We assumed that these ratios varied slowly in radius in accordance with an exponential law with a radial scale length appreciably exceeding L . This choice of velocity dispersion ensured weak instability of the disk at all r . With the exception of specially stipulated cases, we describe below numerical models of “thick” disks.

In none of the models did the velocity dispersion c_r remain constant: the disk “heated up” in the course of its evolution.

²The bending instabilities of the oscillation mode lead to the heating of a thin disk in the vertical direction and, as a result, to its thickening. As our numerical models show, the axisymmetric bending oscillation mode plays an important role.

We found the mean tangential velocity of the model point masses by solving the Jeans equation assuming the absence of systematic radial motions, axial symmetry, and symmetry about the plane $z = 0$:

$$V^2 = (\langle v \rangle)^2 = V_c^2 + c_r^2 \left\{ 1 - \frac{c_\varphi^2}{c_r^2} + \frac{r}{\rho c_r^2} \frac{\partial(\rho c_r^2)}{\partial r} + \frac{r}{c_r^2} \frac{\partial \langle uw \rangle}{\partial z} \right\}, \quad (18)$$

Here, $\langle \dots \rangle$ denotes averaging of the velocities and the last term in (18) is due to the chaotic components of the radial velocity u and vertical velocity w . When specifying the initial state of the model, we assumed that $\langle u \rangle = 0$ and $\langle w \rangle = 0$ and assigned the rotational velocity of the disk in accordance with (18). Thus, initially we have a balance of the radial and vertical forces, and hence the disk begins to evolve from a nearly equilibrium state.

In all the computations, we specified the initial distribution of the velocity dispersion c_φ at $t = 0$ in accordance with (3). We verified that the condition $Q_c \equiv \frac{c_r}{c_\varphi} \frac{\partial}{\partial \Omega} = 1$ was satisfied as the disk evolved. In models with fairly massive halos ($\mu \gtrsim 2$), the mean deviations of Q_c from unit at a given r did not exceed 3% over several dozen rotations of the disk edge. This error is partially due to the numerical differentiation used in a process of computing the epicyclic frequency ∂ . In the models with massive halos, the domain in which $c_r/\partial > r$ is small (for $\mu = 3$, we have $r \lesssim 0.03$). In the case of $\mu \lesssim 1$, this domain expands to $r \lesssim 0.15$. In addition, the vertical disk scale length increases in such models, and these factors result in stronger deviations from the equality (3). The amplitude of fluctuations $Q_c(t)$ decreases as the number of particles increases and does not exceed 2% in models with $\mu \gtrsim 2$ and $N = 2 \times 10^5$ (except for the innermost region of the disk, $r \lesssim 0.5L$), which reflects the *collisionless* nature of the models constructed.

Using the approach described above, we performed more than 40 numerical simulations of the dynamical evolution of a disk toward a steady state in dependence of the initial velocity dispersions $c_r(r)$ and $c_z(r)$. We considered a wide range of parameters for the bulge ($M_b/M_d = 0 \div 3$, $b/L = 0.02 \div 0.8$) and halo ($M_h/M_d = 0 \div 3.5$, $a/L = 1 \div 4$). The number of particles was $N = (40 \div 500) \times 10^3$ in the TREEcode computations.

We verified the stability of the solutions against the choice of computational method by comparing results for several models obtained using two very different methods to compute the gravitational force: the TREEcode method and direct “particle to particle” (PP) integration, in which each particle interacts with each of the other particles, for $N = (20 \div 80) \times 10^3$. As an example, Figure 1 shows the time dependence of the radial-velocity dispersions for one of the models computed using these two methods, with similar initial conditions.³ A comparison of the two results reveals no significant differences between the final disk states.

³The velocity-dispersion components in the plane of the disk c_r and c_φ increase rapidly during the initial stage ($t < 10$) of the heating of an initially cool disk with initial Toomre parameter $Q_T(r < 2L) \simeq 0.85$. The relaxation of the disk in the vertical direction is appreciably slower, so that small local decreases of c_r are possible when the disk is heated in z or there are radial motions (see curve 1 in Fig. 7 after $t > 7$).

5 DETERMINING THE THRESHOLD Q_T VALUES

5.1 Disk Heating Mechanism

An initially axisymmetric, equilibrium disk is heated, increasing its velocity dispersion with time. The question of greatest importance for dynamical simulations is the heating mechanism. To correctly describe the processes in stellar disks, it is important, in particular, to ensure that the heating is not due to the collisional relaxation of the particles, whose number N is many orders of magnitude smaller than the number of stars in real

systems. This is achieved via appropriate choices of the number of particles and the cutoff radius. Our criterion for the absence of significant collisional-relaxation effects is that the character of the system's evolution be preserved when the computations are performed for an increased number of particles, as we verified for many models⁴.

Below, we summarize the most important features of the disk heating shown by the numerical simulations.

(1) The disk-heating time is much greater than the mean rotation period of the particles (Fig. 2a). In the initial stage ($t \lesssim 1$), c_r remains virtually constant, as long as the disk remains axisymmetric. In the case of a low-mass or nonexistent halo, the evolution of the disk is determined by the bar mode, and the disk is heated due to the formation of a nonaxisymmetric bar and associated two-armed spiral. Models with sufficiently massive haloes do not show any enhancement of the bar mode, however they develop a complex transient system of small-scale spiral waves (Fig. 2b). The decrease of the amplitudes of these waves with time is accompanied by the transfer of rotational kinetic energy to the chaotic component of the velocity, resulting in heating of the disk.

(2) The heating of an initially cool disk ($0.5 \lesssim Q_T \lesssim 1$) begins in its central region (Figs. 2a, 2b). The heating at the periphery proceeds much more slowly. The velocity dispersion at the periphery usually begins to rise when the center has already reached a quasi-stationary state (Fig. 2a). At the same time, the processes at the center and at the periphery are interrelated: fast growth of instability in the central region can speed up the heating of the outer part of the disk, while stability of the central region can slow down this process.

3) If the system does not develop a bar, the amplitude of the perturbations begins to decrease with increasing velocity dispersion. In turn, the increase of the radial-velocity dispersion c_r slows down parallel with decreasing wave amplitude. The heating virtually ceases after the decay of the transient spiral waves (see Figs. 2a, 2b). The integrated amplitude of the Fourier harmonics

$$\hat{A}(m; t) = \sqrt{\sum_p A^2(m, p; t)}, \quad A(m, p, t) = \frac{1}{N} \sum_{j=1}^N \exp \{i [m\varphi_j(t) + p \ln(r_j(t))]\}$$

⁴The minimum number of particles N_{crit} for which this criterion is satisfied to sufficient accuracy (i.e., to within random fluctuations of the estimates of the final parameters) depends, in particular, on the form of the rotation curve. The number N_{crit} is larger for highly concentrated nuclei (bulges), due to the higher rotational angular-velocity gradient in the central region of the disk. In the limiting case of a very short, rigidly rotating region, N_{crit} can reach 3×10^6 [20]. Our simulations showed that, if the rotation curve grows monotonically to $r \simeq 2L$, then N_{crit} can be set equal to $\simeq 4 \times 10^4$.

decreases with time for all mode numbers m , but most slowly for $m = 2$ (Fig. 2c). The density distribution in the disk becomes almost axisymmetric (if the mass of the spherical components is large enough to prevent the development of a bar), and, on the whole, the velocity dispersion c_r maintains its level over several dozen rotations, provided that relaxation processes have ceased in the vertical direction.

(4) Whereas three- and even four-armed modes can dominate at the initial stage of evolution of an initially cool disk ($Q_T(r \leq 2L) < 1$; see Figs. 2b, 2c), the spiral pattern changes if we choose a subcritical initial state (i.e., a state that is unstable, but not so cool, where $Q_T \gtrsim 1$). The spatial structure of the perturbations depends to a considerable degree on the relative mass of the spheroidal subsystem. Figure 3 shows the distributions of the logarithm of the disk surface density at various times. The two-armed mode is dominant in this model, although the $m = 3$ harmonic is also important, especially in initial stages of the evolution. It is typical for the spirals to join in the outer region of the disk to form a ring-shaped structure.

(5) Models with low-mass spheroidal subsystems starting from a very cool initial state undergo a substantial mass redistribution in the disk, accompanied by a change in the form of the rotation curve $V(r)$ in the process of heating and formation of a bar. In this case, the final distribution of the surface density $\sigma(r)$ differs strongly from an exponential law (Fig. 4).⁵

Another feature of model disks starting from a very cool initial state ($Q_T \lesssim 1$) is that the velocity dispersion at the end of the computations (after 10–15 rotations) is somewhat higher than is required for gravitational stability. This is due to heating by collective processes—high-amplitude wave motions that develop in the presence of strong instability. When the disk is heated and reaches marginal stability, these perturbations die out, but the wave-decay process has a certain inertia: the velocity dispersion is already high enough to maintain the stability of the disk, but the spiral waves have not yet decayed (as is confirmed by Fourier analysis of the density perturbations in the disk) and continue to heat the disk. Therefore, to obtain the minimum velocity dispersion required for disk stability, we used an iterative algorithm to make the initial velocity dispersion approach the stability limit.

Our *iterative approach* is based on a series of several (two to four) consecutive computations, each of which starts with an initial dispersion that is somewhat closer to the critical level than that for the previous computation. For each radius r , we chose an initial velocity dispersion that was intermediate between the initial and final values (after five to ten rotations) in the previous computation.

As expected, the stability limit also depends on the initial disk thickness⁶. If the disk is

⁵It is possible, in principle, to choose an initial density profile that yields an exponential profile at the end of the computations (dashed line in Fig. 4); however, this approach is rather artificial. It seems that the stellar disks of most of the galaxies do not pass through a stage of strong dynamical instability.

⁶The initial thicknesses of the disks of real galaxies depend on the conditions under which they were formed. For example, if the collapse of a gaseous disk was accompanied by violent star formation before it reached a quasi-stationary state, the resulting stellar disk may be much thicker and have a higher velocity dispersion c_z than the minimum value required for stability. However, such a scenario is difficult to reconcile with the existence of very thin ($h_z/L < 0.2$) stellar disks in edge-on galaxies. The dependence of the disk thickness on the relative mass of the halo is also consistent with the assumption that the stellar-velocity dispersion is close to the value expected for

initially thick (with the vertical scale height $h_z \gtrsim 0.2L$) and unstable only in its plane ($c_r < c_r^{\text{crit}}$), its heating proceeds more slowly and ceases at lower radial-velocity dispersions than in the case of an initially thin disk. This is due to two factors: the stabilizing effect of the finite thickness of the disk and the slowness of the relaxation in the vertical direction compared to the heating in the plane of the disk.

The results of dynamical simulations allow to determine the disk parameters at the gravitational-stability limit (when the velocity dispersion ceases to change, after $5 \div 20$ rotations of the outer edge of the disk).

5.2 Gravitational-Stability Threshold for Bulgeless Models

We computed a series of bulgeless galaxy models, differing in the relative mass $\mu = M_h/M_d$ and the halo scale length a , with a fixed radial disk scale L .

When $a \gtrsim L$, the rotation curve has an extended section $V_c(r)$ (which we will call the “rigid-rotation” section), which makes a transition to a plateau $V_c \simeq \text{const}$ at $r \gtrsim 2L$ (curve 1 in Fig. 5a). Figure 5a shows for a bulgeless galaxy with $\mu = 1$ the radial distributions of the circular rotational velocity $V_c(r)$ (curve 1), mean particle rotational velocity $V(r)$ (curve 2), radial-velocity dispersion $c_r(r)$ (curve 3), and the differential-rotation parameters $S = 2\Omega/\alpha$ computed separately for $V_c(r)$ and $V(r)$ (4 and 5).

Knowing the final velocity dispersions, disk density, and rotational velocity, it is possible to compare the Toomre stability parameters Q_T (1) for the corresponding model with the analytically derived local criteria discussed above and compare these criteria with each other. Note that the analytical criteria were derived assuming that the circular rotational velocity $V_c(r)$ differs little from the mean velocity $V(r)$ of the gravitating point masses. However, the difference between these velocities can be quite significant for collisionless disks. We therefore determined the stability parameters for both $V_c(r)$ and $V(r)$.

Figure 5b shows for this model the computed Q_T and the Toomre parameters required for marginal stability according to the criteria of Polyachenko, Polyachenko, and Strel’nikov (PPS) $Q_T^{(P)}$ (6) and Morozov $Q_T^{(M)}$ (5) calculated separately using the circular velocity and the mean rotational velocity of the particles. In the case of a massive halo ($\mu \gtrsim 2$), the difference between the stability parameters for $V_c(r)$ and $V(r)$ is small, but it can become appreciable for $\mu \lesssim 1$ (Figs. 5a, 5b). This is due to the fact that the difference $V_c - V$ increases with increasing velocity dispersion in accordance with (18).

The condition $S \simeq Q_T^{(M)} \lesssim Q_T \lesssim Q_T^{(P)}$ is satisfied both in the case considered here and for most of the models (recall that $Q_T = S$ is the Toomre condition for marginal stability with crude allowance for nonaxisymmetric perturbations; see Section 2).

Figures 5c and 5d compare the stability criteria in a different way. These figures show the radial dependences of the ratio of the model velocity dispersion c_r of the disk when it becomes stable to the critical velocity dispersion for the various criteria considered in Section 2. A perfect agreement with the model

dependences would correspond to the ratio $c_r/c_{\text{crit}} = 1$.

Although none of the criteria explain the model dependences $Q_T(r)$ at all r , the closest results are given by the PPS criterion generalized for the case of finite thickness (2) and the Morozov criterion (5) (symbols 15 and 16 in Fig. 5c). When the stability criteria are determined in terms of the mean rotational velocity (Fig. 5b), the radial variations of c_r/c_{crit} conserve their general form (Fig. 5d). Note that for the interval $0.1 < r < 0.8$ the ratio c_r/c_{crit} is closest to unity for the Morozov criterion (curve 16). It is striking that the PPS criterion (curve 12) overestimates c_{crit} in all cases, but c_r/c_{crit} remains nearly constant over a wide range of r , enabling easy introduction of a correction factor for c_{crit} .

The important result is that the radial dependence of the Toomre parameter $Q_T(r)$ computed for the circular velocity $V_c(r)$ shows qualitatively similar behavior for all the bulgeless models we considered (Fig. 5e). Moreover, $Q_T(r)$ remains approximately constant at the level $Q_T \simeq 1.2 \div 1.6$ in the interval $0 \lesssim r/L \lesssim 2$ (see Fig. 5e). At the disk periphery ($r \gtrsim 2L$), Q_T increases with radius, reaching $Q_T \simeq 2.5 \div 3$ at the edge of the disk ($r \simeq 4L$). However, the scatter of the Q_T values for the various models is small, enabling us to adopt the following function as a lower envelope

$$Q_T^{(*)} = A_0 + A_1 \cdot \left(\frac{r}{L}\right) + A_2 \cdot \left(\frac{r}{L}\right)^2, \quad (19)$$

where $A_0 = 1.25$, $A_1 = -0.19$, and $A_2 = 0.134$ (bold curve in Fig. 5e). This function reaches its minimum, equal to 1.2, at $r/L = 0.7$.

The observational estimates of the stellar-velocity dispersions are usually based on data for the inner region of the disk $r < 2L$. Therefore, the approximate constancy of Q_T in this region makes this quantity a convenient tool for estimating the surface density and mass M_d of a disk (assuming it is stable) based on the known rotation curve of the galaxy and the radial exponential disk scale length L . The equation relating these quantities is

$$c_r = Q_T^{(*)}(r) \frac{3.36G\sigma_0 \exp(-r/L)}{\varkappa}, \quad (20)$$

where $Q_T^{(*)}$ for galaxies with the extended region of increasing $V_c(r)$ is determined by (19). In turn, the disk mass estimate $M_d = 2\pi\sigma_0 L^2$ makes it possible to separate out the mass of the dark halo within a specified radius.

5.3 Models with Formation of a Bar

In the case of a low-mass or very “loose” halo and no bulge, the evolution of an initially cool dynamical model inevitably results in the development of a bar. As a rule, the formation of a bar involves an appreciable radial redistribution of the mass, whose intensity increases when the velocity dispersion in the initial state decreases. The outer boundary of the disk shifts outward. As a result, the radial scale for the azimuthally averaged surface density $L = -(d \ln \sigma / dr)^{-1}$ varies, which can lead to deviations from an exponential profile (when $L = \text{const}$ throughout the disk). In the innermost region ($r \lesssim 0.3L$), the surface density can increase appreciably over its initial value (Fig. 4), bringing about a decrease of Q_T in accordance with (1). A similar conclusion concerning the increase in the central density during the formation of a bar was also reached for models with “living” (evolving) haloes [55]. Numerical simulations have shown that, under certain conditions,

the interaction between the bar and “living” halo can appreciably affect the dynamical evolution of the bar [56].

The stability criteria considered above were derived for and applied to axisymmetric disks. However, it is of interest to formally compute these criteria based on azimuthally averaged parameters in the absence of axial symmetry in the inner region — that is for barred galaxies. As an example, Figure 6 shows the radial distributions of the parameters of a disk that has developed a bar (Figs. 6a–6c show results for a model with a low-mass halo and Figs. 6d–6f results for a model with a halo whose initial mass within $r = 4L$ is twice that of the disk). The radial distributions of the surface density in the bar region can differ from those outside the bar (Figs. 6c, 6f). The development of a bar usually results in additional thickening of the disk. The function $Q_T(r)$ depends on the bar parameters (essentially, on the initial conditions), however for $r \gtrsim L$ the condition $Q_T \gtrsim 1.5$ is satisfied, and the radial dependence $Q_T(r)$ is qualitatively similar to that observed for an axisymmetric disk. The development of a bar in models with more massive haloes is accompanied by weaker deviations from the initial exponential surface-density profile (Fig. 6f).

The characteristic dependences for the model with a massive halo (Figs. 6d–6f) differ little from the cases shown in Fig. 5 for barless models. As expected, suppressing the bar mode requires a higher initial velocity dispersion c_r or a more massive halo, in accordance with classical concepts (see, e.g., [29, 44]).

5.4 Models with Bulges

Let us consider now model galaxies whose rotation curves in the central region ($r \lesssim L$) are determined primarily by the bulge. As a rule, the rotations curves outside the bulge ($r \gtrsim L$) are almost flat ($V \simeq \text{const}$). Figure 7 shows typical model radial dependences of the disk parameters for this case. In the presence of a bulge, Q_T increases strongly in the central region of the disk, where the dynamics are determined by the bulge potential (Figs. 7b, 7e). However, outside this region, at $r \simeq (1 \div 2) \times L$, the radial dependence of Q_T retains its form [see (19), Fig. 5e]. At larger distances Q_T increases monotonically with r up to values $2.5 \div 3.5$. The resulting radial dependence of Q_T is typical of systems with bulges that are not too massive ($M_b/M_d \lesssim 0.3$) and not very extended ($(r_b)_{\text{max}} \lesssim L$).

The more massive and more compact the bulge, the higher the value of Q_T at the disk center. This increase of the Toomre parameter is due mainly to the growth of the epicyclic frequency α . The radial-velocity dispersion in the central region also increases somewhat with increasing mass of a strongly concentrated bulge. Additional heating of the center of the disk ($r \lesssim 0.5L$) in the model shown in Fig. 7a has no direct connection with gravitational instability. At the initial stage of its evolution, this model, where $\mu = 1$, a bar develops, which disappears soon as a result of scattering of particles passing near the concentrated nucleus (the latter has a scale length $b = 0.01$). This mechanism for bar disruption is similar to the effect produced by a black hole [57].

As a result, the disk undergoes additional heating and becomes thicker in the central region (Fig. 7f). The degree of this additional heating and the circular velocity V_c at the disk center are very sensitive to the bulge parameters, first and foremost, the core radius b (in particular, the bar disruption mentioned above does not take place if $b \gtrsim 0.05L$). Therefore, at $r \lesssim 0.5L$ the Toomre parameter Q_T can vary very strongly in different models (Fig. 7f).

5.5 Differential Rotation as a Factor Increasing the Threshold for Gravitational Stability

Here we consider two limiting cases: a disk that rotates almost rigidly and a quasi-Keplerian disk whose rotational velocity decreases as $V \propto r^{-1/2}$. Since differential rotation is a destabilizing factor, rigidly rotating disks are expected to have lower Q_T , other conditions being the same.

Galaxies usually exhibit an extended interval of almost rigid body rotation if the mass of the disk dominates throughout most of the disk ($r \lesssim 2L$), so that suppression of the bar instability requires stronger disk heating than in the presence of massive spherical components. Therefore, to elucidate the role of differential rotation, we analyzed a model in which the development of a bar is suppressed by a massive halo, yet the outer part of the disk ($r \gtrsim L$) contains a rigidly rotating section. The differential-rotation parameter in this model $S(r > L) = 2\Omega/\alpha = 1.1 \div 1.2$ is close to $S = 1$, which corresponds to completely rigid rotation (Fig. 8a). Figure 8a shows the radial dependences of Q_T , $Q_T^{(P)}$, $Q_T^{(M)}$, and S characterizing the stability of the system. It is clear that, in general, the disk becomes stable at lower values of Q_T (curve 6) than in the cases considered above. In this case we have $Q_T \simeq 1$ and $Q_T \simeq 2$ at the disk center and periphery, respectively.

Consider now another limiting case, corresponding to a nearly Keplerian rotation curve (Fig. 8b). Such behavior is very rarely seen in the rotation curves of real galaxies, but we are interested in the fundamental question of how strong differential rotation affects the minimum velocity dispersion required for stability. To produce quasi-Keplerian disks, we introduced massive concentrated components into our dynamical model. The resulting series of models is a natural extension of those with very massive bulges ($M_b > (2 \div 4)M_d$). Figure 8b shows the results obtained for one of such models. The Toomre parameter increases appreciably for disks with strong differential rotation, so that the condition $Q_T > 2$ is necessary for stability, even in the region where Q_T is minimal ($r \simeq (1 \div 2)L$).

Since the central region is dominated by the spheroidal system, no bar develops, and there is no increase in the velocity dispersion there, which was mentioned in Section 5.4 (Fig. 7a).

6 DISCUSSION AND CONCLUSIONS

We have carried out numerical simulations of the evolution of disks that are initially unstable, collisionless, and in equilibrium for a whole series of three-dimensional models. The aim of our analysis was to compare the minimum radial-velocity dispersions c_r at which the disks reach their final, quasi-stationary state (as a rule, after 5–10 rotations of the outer edge of the disk) with the velocity dispersion $c_T = 3.36\pi G\sigma/\alpha$ required to suppress gravitational instability of a thin disk against axially symmetrical perturbations (the Toomre criterion), as well as with other local stability criteria. We separately analyzed the influence of the bulge, dark halo, differential rotation, and initial disk parameters on the radial behavior of $Q_T = c_r/c_T$.

Our numerical simulations show that differential rotation and inhomogeneity of the disk, the global nature of perturbations, and the finite thickness of the disk can change the local velocity dispersions (or the local Toomre parameters) of marginally stable disks by $\gtrsim 50\%$. The numerical models enable to carry out a separate analysis of the effects of each of these factors.

The models considered here clearly demonstrate rapid heating of initially unstable disks during the formation and destruction of transient spiral arms. The low-contrast “remnants” of these arms can be traced over more than ten rotations. A similar character of disk evolution we obtained for models which used both different numbers of particles and a different computational algorithm (PP method).

As expected, the minimum radial-velocity dispersion at the end of the simulations (expressed in units of the circular velocity) is higher in the models where the relative mass of the halo is lower, the initial disk thickness is less, and the degree of differential disk rotation is higher. Although the radial dependence of Q_T differs for different models and is determined primarily by the relative mass and degree of concentration of the spherical components, in all cases, $Q_T(r)$ passes through a minimum $Q_T \simeq 1.2 \div 1.6$ at a galactocentric distance of $(1 \div 2)L$, and this behavior depends only slightly on the choice of model. This fact can be used to approximately estimate the density (and, consequently, the mass) of a galactic disk (or to put limits on these quantities) from observed radial-velocity dispersions using equations (19) and (20) without the use of numerical simulations or analytical stability criteria. If the halo is not too massive ($M_h/M_d \lesssim 2$), a disk that begins its evolution from a strongly unstable state rather than from a subcritical state can experience a substantial mass redistribution over one or two rotations. The fact that galaxies usually have exponential brightness distributions indicates that the formation of stellar disks, apparently, was not accompanied by the development of strong gravitational instability.

The thicker is the disk initially, the lower is the minimum radial velocity dispersion c_r , which determines its stability. Therefore, the minimum critical dispersions in both coordinates z and r are reached if the disk begins to evolve from a subcritical state. It’s valid both for gravitational perturbations in the plane and for bending perturbations (global, primarily axisymmetric mode, and small-scale ones).

The disk evolution traced by the numerical models clearly demonstrates the interrelations of processes at different r . Initial stability of the central disk region slows down while strong initial instability accelerates the increase of the velocity dispersion at the disk periphery, having, however, no significant effect on the final state.

Existing analytical criteria for the stability of thin disks are based on other considerations, and, strictly speaking, there is no reason why they must coincide with the Q_T values we have found, due to the local nature of the criteria applied, as well as due to the use of two-dimensional analytical models, while dynamical models treat the disk heating in three dimensions. The model velocity dispersions differ significantly from those predicted by various criteria (Figs. 5b–5d, 6b, 6e, 7b–7d, 8a, and 8b). However, it’s evident that the formal application of these criteria will yield results that are correct to order of magnitude. In particular, like model estimates, they imply that $Q_T > 1$ at all r and that this parameter increases at the disk periphery. However, in none of the cases considered do the $Q_T(r)$ relations derived using local criteria agree with those found in this work for all radial distances ($0 < r < 4L$), and that they can differ from the model estimates by more than a factor of 1.5 at some distances r .

After passing through its minimum, the Toomre parameter $Q_T(r)$ for a disk that has reached a stable equilibrium state increases monotonically with r up to $Q_T \simeq 2 \div 3$ at a radius of $(3 \div 4)L$ (this radius is usually close to the optical boundary of the disk in real galaxies). Note that a similar increase of $Q_T(r)$ from 1.5 to 2.5 at the periphery was obtained earlier by Pichon and Lynden-

Bell [49] using a different method (by constructing stable equilibrium distribution functions for flat systems over a wide range of free parameters) and has also been mentioned for a number of dynamical models [5, 21, 24, 44–47].

The disks of galaxies whose halo are not too massive ($\mu \lesssim 1.5$) are subjected to bar instability. The suppression of the development of a long-lived bar in galaxies with low-mass spherical components requires not only a higher velocity dispersion (as shown long ago by Ostriker and Peebles [29] in their classic work) but also a higher value of the Toomre parameter Q_T , compared to galaxies possessing a massive halo or bulge. Moreover, the development of a bar is accompanied by an increase in Q_T even in regions of the galaxy beyond the bar. This effect is apparently associated with the system being “overheated” above the threshold level: the development of the bar is accompanied by a redistribution of mass in the disk, so that the local decrease of the disk surface density for the given velocity dispersion results in an additional increase in Q_T . However, in this case, our models fail to yield *bona fide* quantitative estimates, since the parameters of the bar depend strongly on the initial conditions in the system. We have not analyzed here the conditions for the development of the bar mode in detail.

Our results make it possible to use numerical models to estimate the degree of dynamical heating of stellar disks and to derive estimates for the *a priori* unknown mass and density of a galactic disk from the observed velocity dispersion of the old stars making it up.

7 ACKNOWLEDGMENTS

We are grateful to A.M. Fridman, O.V. Khoruzhiĭ, and V.L. Polyachenko for useful discussions of this work and comments. This work was supported by the Russian Foundation for Basic Research (project no. 01-02-17597) and partially supported by the Federal Research and Technology Program “Research and Development in Priority Fields of Science and Technology” (contract 40.022.1.1.1101).

References

- [1] A. Toomre, *Astrophys. J.* **139**, 1217 (1964).
- [2] A. G. Morozov, *Astron. Zh.* **58**, 734 (1981) [*Sov. Astron. Rep.* **25**, 421 (1981)].
- [3] A. V. Zasov, *Pis'ma Astron. Zh.* **11**, 730 (1985) [*Sov. Astron. Lett.* **11**, 307 (1985)].
- [4] R. Bottema, *Astron. Astrophys.* **275**, 16 (1993).
- [5] R. Bottema and J. P. E. Gerritsen, *Mon. Not. R. Astron. Soc.* **290**, 585 (1997).
- [6] B. Fuchs, in *Galaxy Dynamics*, ASP Conf. Ser. **182**, Ed. by R. D. Merritt, M. Valluri, and J. A. Sellwood (Astronomical Society of the Pacific, San Francisco, 1999), p. 365.
- [7] A. V. Khoperskov, A. V. Zasov, and N. V. Tyurina, *Astron. Zh.* **78**, 213 (2001) [*Astron. Rep.* **45**, 180 (2001)]; A. V. Zasov, D. V. Bizyaev, D. I. Makarov, and N. V. Tyurina, *Pis'ma Astron. Zh.* **28**, 599 (2002) [*Astron. Lett.* **28**, 527 (2002)].

- [8] A. M. Fridman and V. L. Polyachenko, *Physics of Gravitating Systems* (Springer-Verlag, New York, 1984).
- [9] V. L. Polyachenko and A. M. Fridman, *Equilibrium and Stability of Gravitating Systems* [in Russian] (Nauka, Moscow, 1976).
- [10] N. N. Gor'kavyĭ and A. M. Fridman, *Physics of Planetary Rings* [in Russian] (Nauka, Moscow, 1994).
- [11] C. C. Lin and F. H. Shu, *Astrophys. J.* **140**, 646 (1964).
- [12] O. P. Vandervoort, *Astrophys. J.* **161**, 87 (1970).
- [13] A. G. Morozov, *Astron. Zh.* **57**, 681 (1980) [*Sov. Astron. Rep.* **24**, 397 (1980)].
- [14] A. G. Morozov and A. V. Khoperskov, *Astrofizika* **24**, 467 (1986).
- [15] E. Griv, C. Yuan, and M. Gedalin, *Mon. Not. R. Astron. Soc.* **307**, 1 (1999).
- [16] A. G. Morozov, *Pis'ma Astron. Zh.* **7**, 197 (1981) [*Sov. Astron. Lett.* **7**, 109 (1981)].
- [17] V. L. Polyachenko, E. V. Polyachenko, and A. V. Strel'nikov, *Pis'ma Astron. Zh.* **23**, 598 (1997) [*Astron. Lett.* **23**, 525 (1997)].
- [18] N. W. Evans and J. C.A. Read, *Mon. Not. R. Astron. Soc.* **300**, 83 (1998).
- [19] N. W. Evans and J. C. A. Read, *Mon. Not. R. Astron. Soc.* **300**, 106 (1998).
- [20] J. A. Sellwood and N. W. Evans, *Astrophys. J.* **546**, 176 (2001).
- [21] G. Bertin, C. C. Lin, S. A. Lowe, and R. P. Thurstans, *Astrophys. J.* **338**, 78 (1989).
- [22] R. H. Miller, *Astrophys. J.* **223**, 811 (1978).
- [23] R. H. Miller, K. H. Prendergast, and W. J. Quirk, *Astrophys. J.* **161**, 903 (1970).
- [24] F. Hohl, *Astrophys. J.* **168**, 343 (1971).
- [25] F. Hohl, *Astron. Space Sci.* **14**, 91 (1971).
- [26] R. H. Miller, *Astron. Space Sci.* **14**, 73 (1971).
- [27] R. H. Miller, *Astrophys. J.* **190**, 539 (1974).
- [28] R. H. Miller, *Astrophys. J.* **223**, 811 (1978).
- [29] J. P. Ostriker and P. J.E. Peebles, *Astrophys. J.* **186**, 467 (1973).
- [30] R. A. James and J. A. Sellwood, *Mon. Not. R. Astron. Soc.* **182**, 331 (1978).
- [31] V. L. Polyachenko and I. G. Shukhman, Preprint Nos. 1–2, SIBIZMIR, Sib. Div. Akad. Nauk SSSR (1972).
- [32] A. J. Kalnajs, *Astrophys. J.* **175**, 63 (1972).
- [33] E. A. Mikhaĭlova and A. V. Khoperskov, *Astron. Zh.* **69**, 1112 (1992) [*Astron. Rep.* **36**, 573 (1992)].
- [34] E. Athanassoula and J. A. Sellwood, *Mon. Not. R. Astron. Soc.* **221**, 213 (1986).

- [35] C. J. Jog and P. M. Solomon, *Astrophys. J.* **276**, 114 (1984).
- [36] C. J. Jog and P. M. Solomon, *Astrophys. J.* **276**, 127 (1984).
- [37] B. Wang and J. Silk, *Astrophys. J.* **427**, 759 (1994).
- [38] V. G. Ortega, E. Volkov, and L. Monte-Lima, *Astron. Astrophys.* **366**, 276 (2001).
- [39] J. A. Sellwood and R. G. Carlberg, *Astrophys. J.* **282**, 61 (1984).
- [40] R. G. Carlberg and J. A. Sellwood, *Astrophys. J.* **292**, 79 (1985).
- [41] J. A. Sellwood and E. Athanassoula, *Mon. Not. R. Astron. Soc.* **221**, 195 (1986).
- [42] J. A. Sellwood, *Mon. Not. R. Astron. Soc.* **238**, 115 (1989).
- [43] J. A. Sellwood and D. N.C. Lin, *Mon. Not. R. Astron. Soc.* **240**, 991 (1989).
- [44] J. A. Sellwood and E. Athanassoula, in *Internal Kinematics and Dynamics of Galaxies*, (Reidel, Dordrecht, 1983), p. 203.
- [45] H. C. Schroeder and N. F. Comins, *Astrophys. J.* **346**, 108 (1989).
- [46] B. Fuchs and S. von Linden, *Mon. Not. R. Astron. Soc.* **294**, 513 (1998).
- [47] J. M. Bardeen, *IAU Symp. 69: Dynamics of Stellar Systems*, Ed. by A. Hayli (D. Reidel, Dordrecht, 1975), p. 297.
- [48] A. V. Zasov, A. G. Morozov, *Astron. Zh.* **62**, 475 (1985) [*Sov. Astron. Rep.* **29**, 277 (1985)].
- [49] C. Pichon and D. Lynden-Bell, *Mon. Not. R. Astron. Soc.* **282**, 1143 (1996).
- [50] A. B. Romeo, *Astron. Astrophys.* **286**, 799 (1994).
- [51] A. B. Romeo, *Astron. Astrophys.* **335**, 922 (1998).
- [52] J. Sommer-Larsen, H. Vedel, and U. Hellsten, *Mon. Not. R. Astron. Soc.* **294**, 485 (1998).
- [53] J. C. Lambert and A. Bosma, *Mon. Not. R. Astron. Soc.* **314**, 475 (2000).
- [54] J. N. Bahcall, *Astrophys. J.* **276**, 156 (1984).
- [55] E. Athanassoula and A. Misiriotis, *Mon. Not. R. Astron. Soc.* **330**, 35 (2002).
- [56] V. P. Debattista and J. A. Sellwood, *Astrophys. J.* **543**, 704 (2000).
- [57] H. Hasan and C. Norman, *Astrophys. J.* **361**, 69 (1990).

Translated by A. Dambis

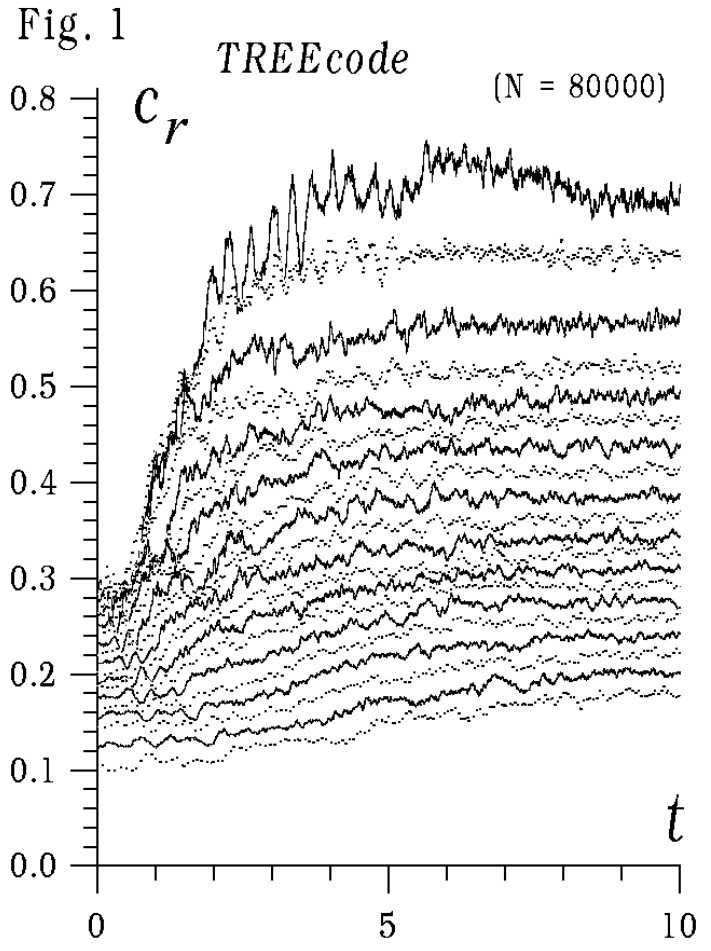
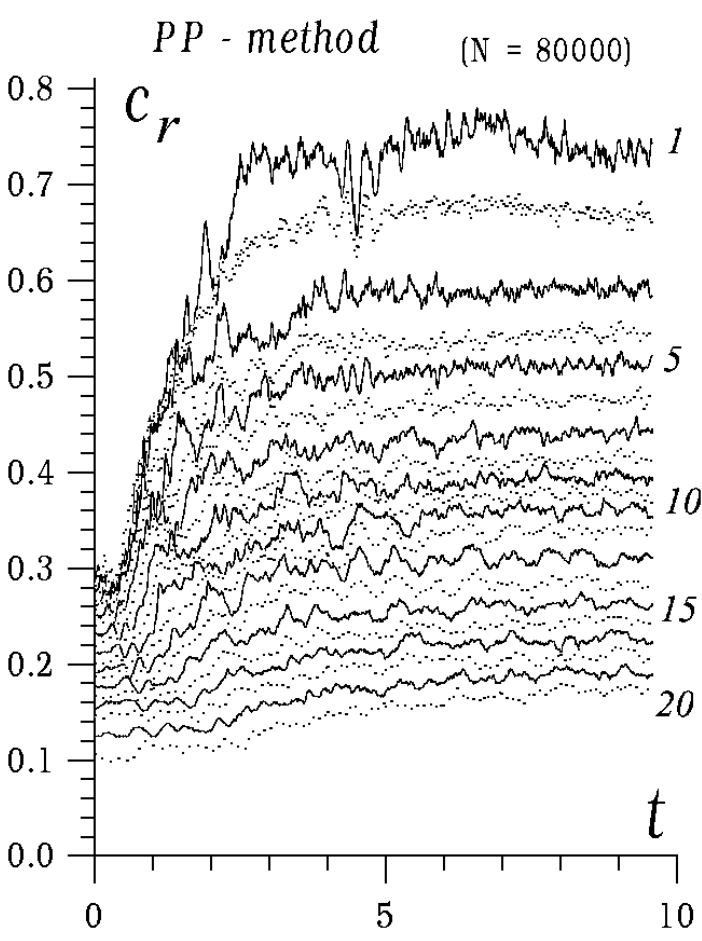


Figure 1. Time dependence of the radial-velocity dispersion $c_r(r)$ for particles at 20 different galactocentric distances (1 is the central zone, and each zone has a width of $0.05R$) at the initial stage of heating of a cool, thin disk ($t = 10$ corresponds to ~ 3 rotations of the outer edge of the disk) for two methods of computing the gravitational force with $N = 80\,000$: (a) the PP algorithm and (b) the TREE-code algorithm.

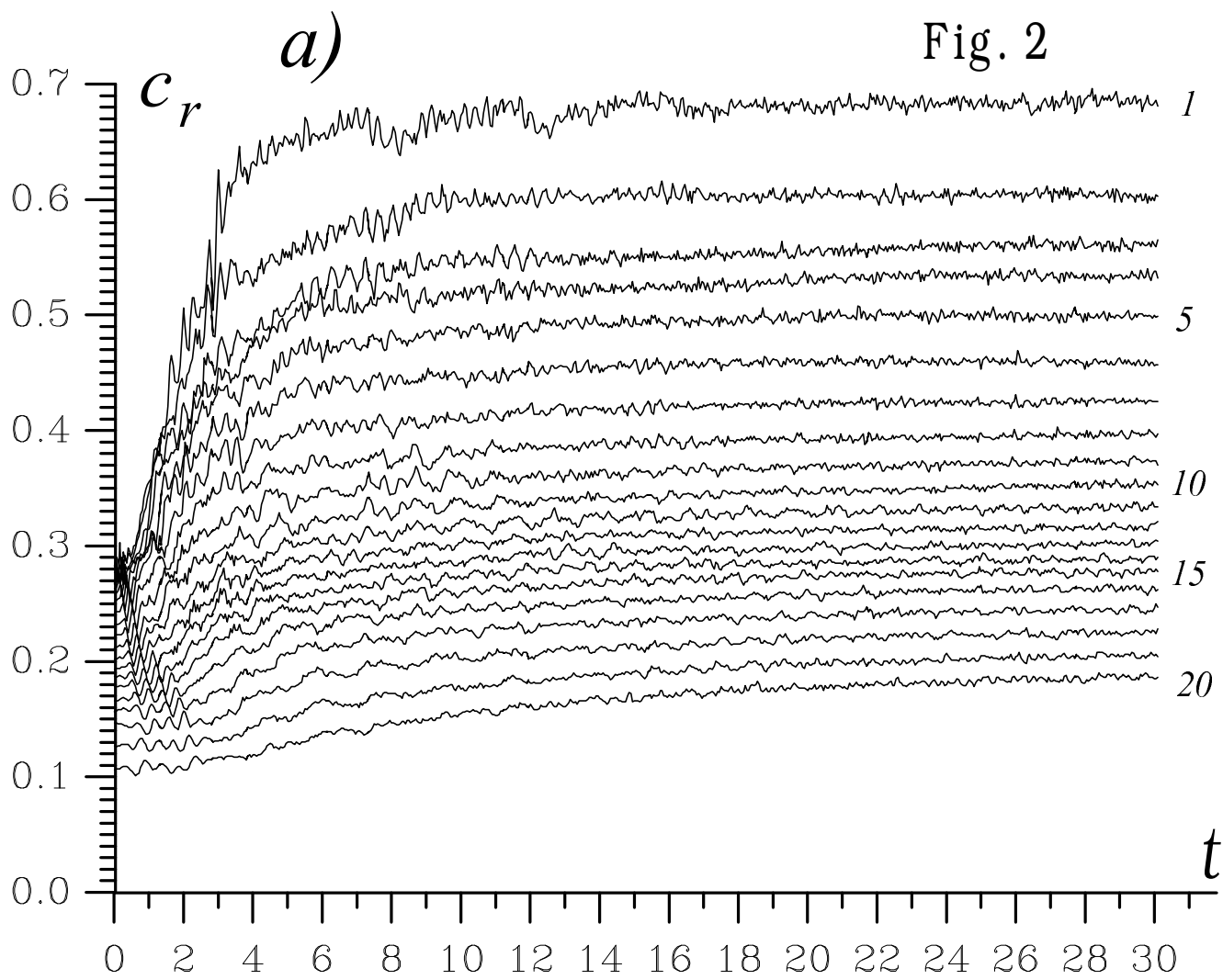
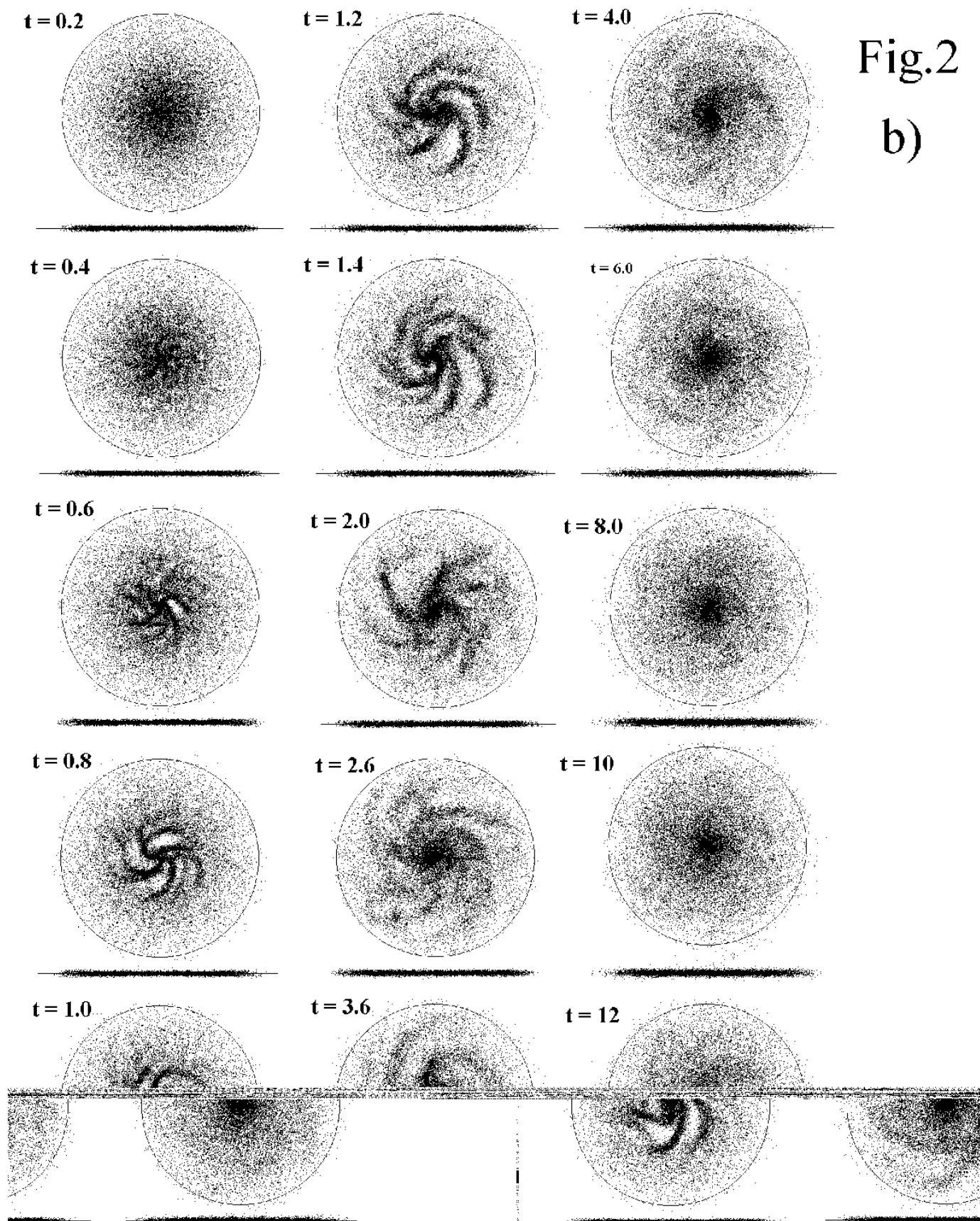


Figure 2. Evolution of an initially unstable thin disk ($\mu = 3$, $a = L$). (a) Time dependence of the radial-velocity dispersion in 20 radial zones. (b) Development of a system of transient spiral waves in an initially axisymmetric disk. The positions of point masses in the (x, y) plane at various times are presented (since the model consists of 5×10^5 particles, only some of the point masses are shown). (c) Time dependence of the integrated amplitudes $\hat{A}(m)$ of the Fourier harmonics for various modes $m = 2, \dots, 6$. The parameters \hat{A} reach their maximum values at $1 \lesssim t \lesssim 4$, and it is in this time interval that the perturbations reach their maximum amplitudes (Fig. 1b). After $t > 4$, \hat{A} decreases, which corresponds to the beginning of wave dissipation and the slowing down of the growth of c_r (Fig. 2a).



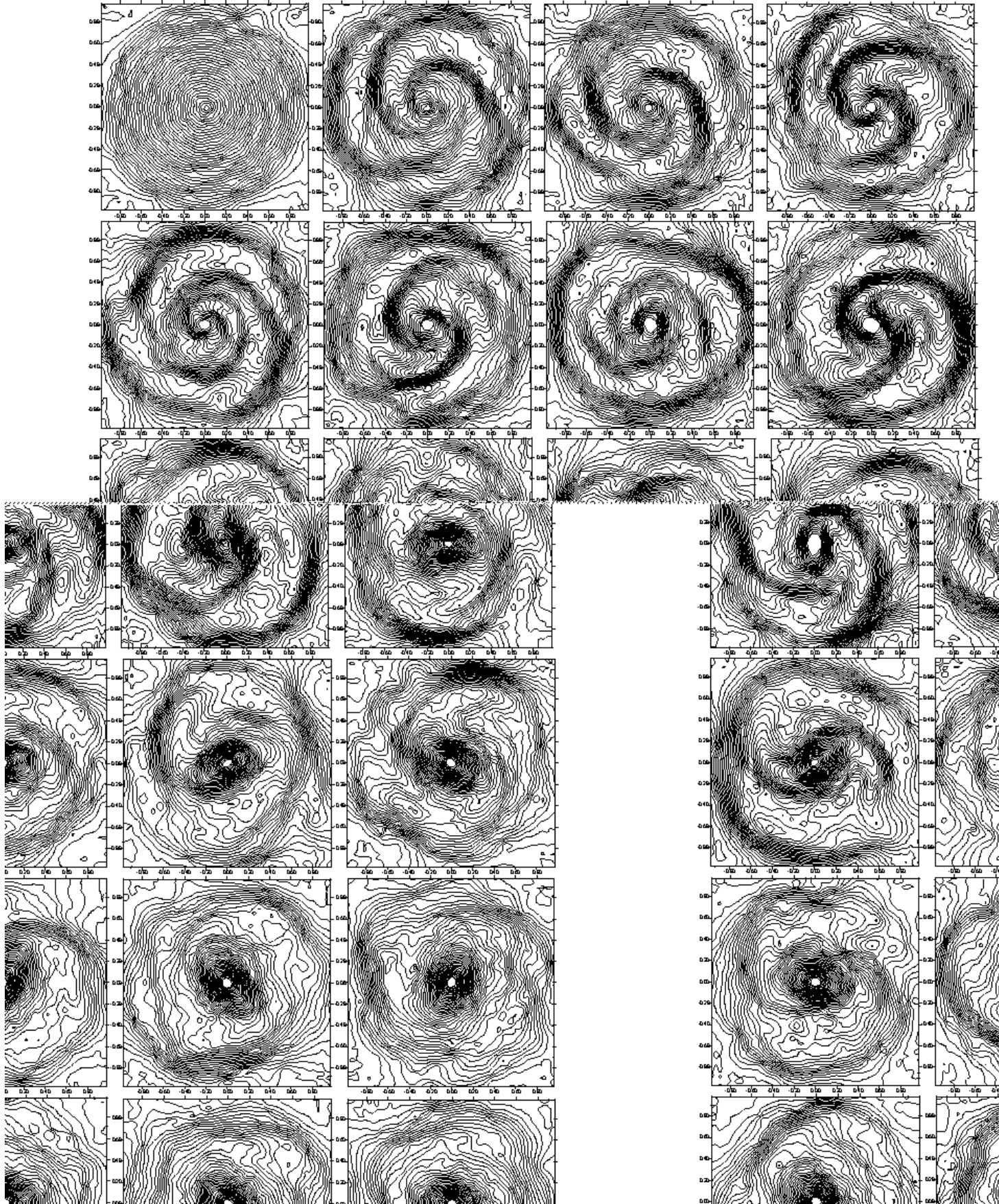


Figure 3. Distribution of the logarithmic surface density $\log \sigma$ at various times from $t = 1$ to $t = 30$ for the initial subcritical state with $Q_T \gtrsim 1$.

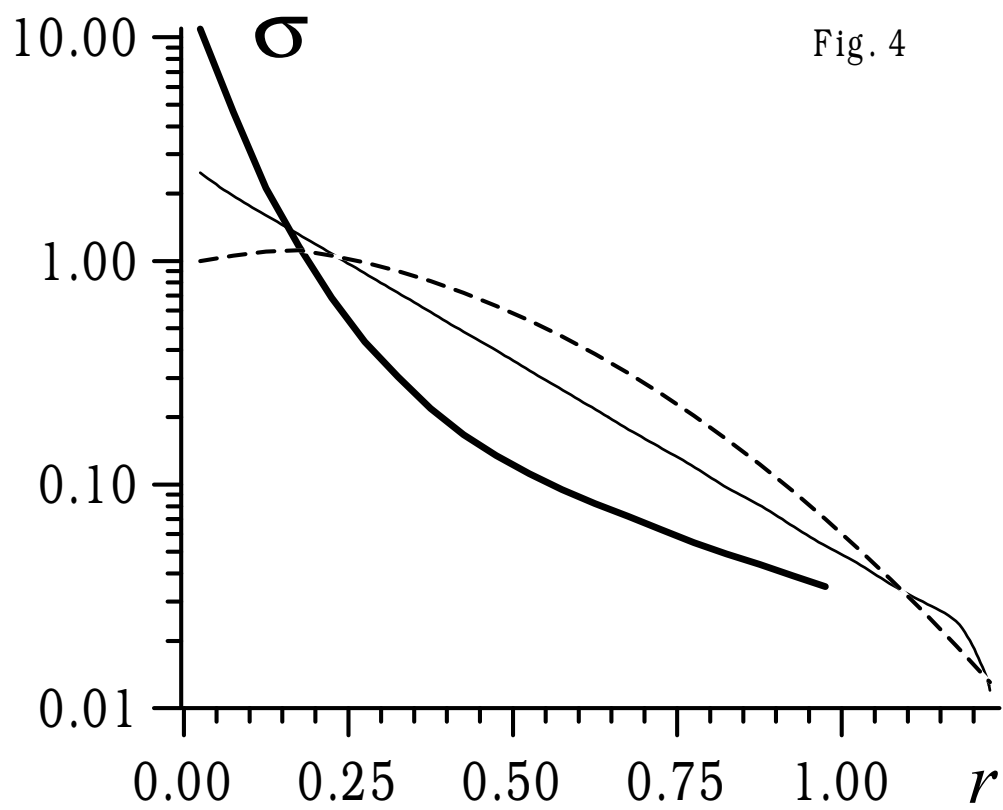


Fig4. Radial dependences of the surface density for an initially cool model disk in which there is subsequently a substantial density redistribution. The thin solid curve shows an exponential profile, the bold solid curve is the final profile averaged in azimuth after strong heating and development of a bar, and the dashed curve is the initial profile that produces a quasi-exponential distribution at the end of the computations.

Fig. 5

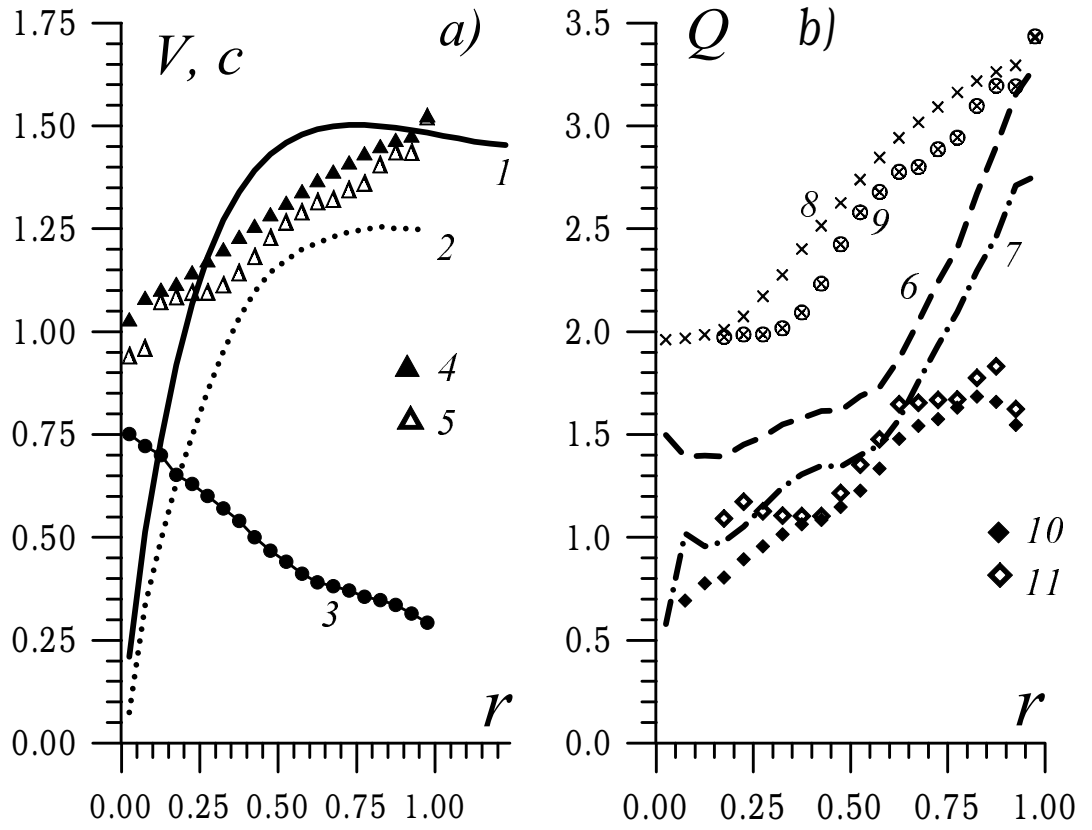


Fig.5. Parameters of the disk that has evolved to a stable state at the stability limit, for bulgeless models. (a) Radial dependences of the circular velocity $V_c(r)$ (curve 1), disk rotational velocity $V(r)$ (curve 2), radial-velocity dispersion $c_r(r)$ (curve 3), and parameters $S = 2\Omega/\alpha$ computed for the circular velocity (curve 4) and disk rotational velocity (curve 5), respectively. Results are shown for the model in which the mass of the halo within $r \leq 1 = 4L$ is equal to that of the disk and the halo scale length a is equal to the radial disk scale length L . (b) Radial dependences of the Toomre parameter at the stability limit computed using various stability criteria for the model shown in Fig. 5a: 6 Q_T determined from V_c , 7 Q_T determined from V , 8 $Q_T^{(P)}$ determined from V_c , 9 $Q_T^{(P)}$ determined from V , 10 $Q_T^{(M)}$ determined from V_c , and 11 $Q_T^{(M)}$ determined from V .

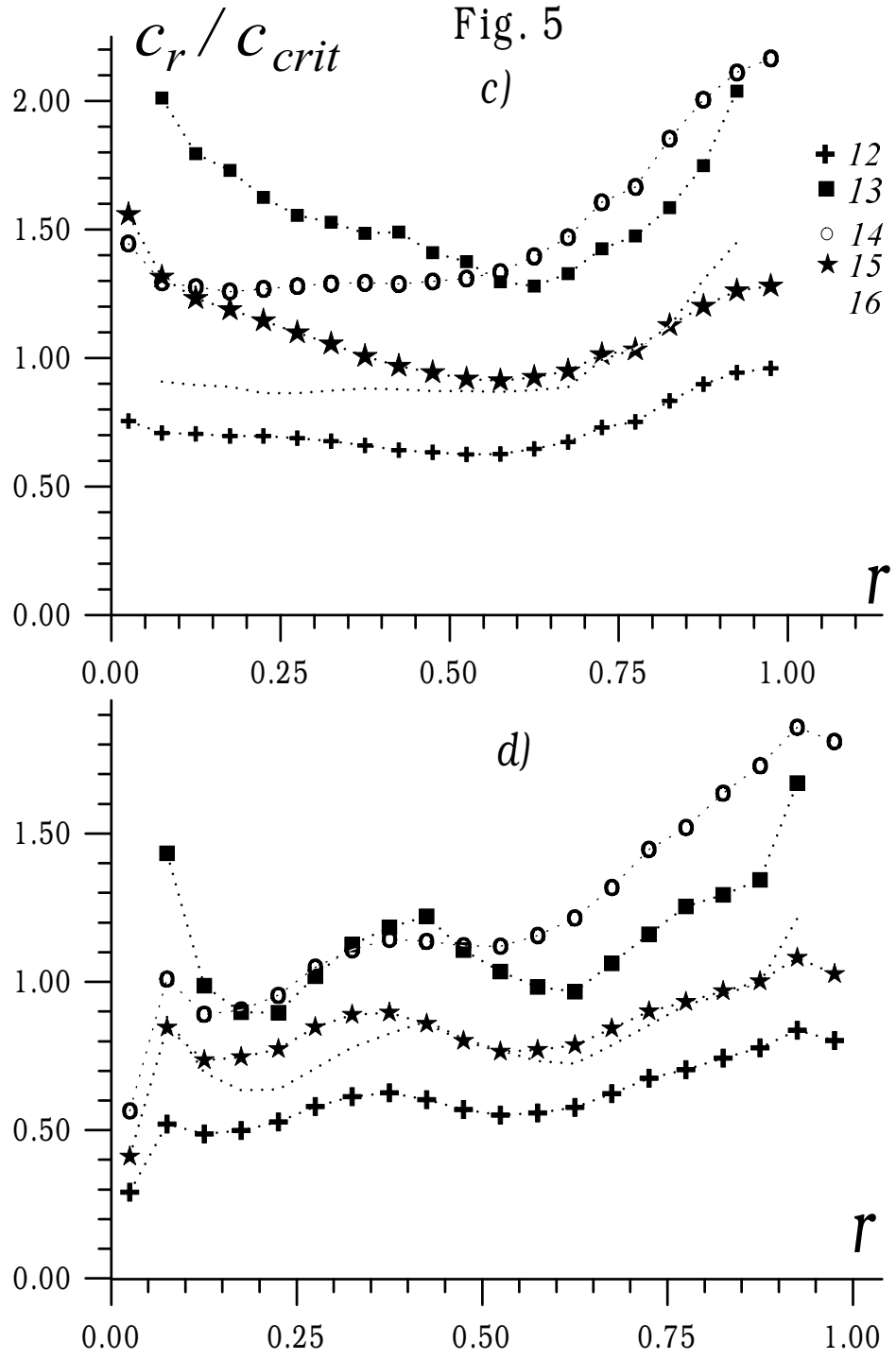
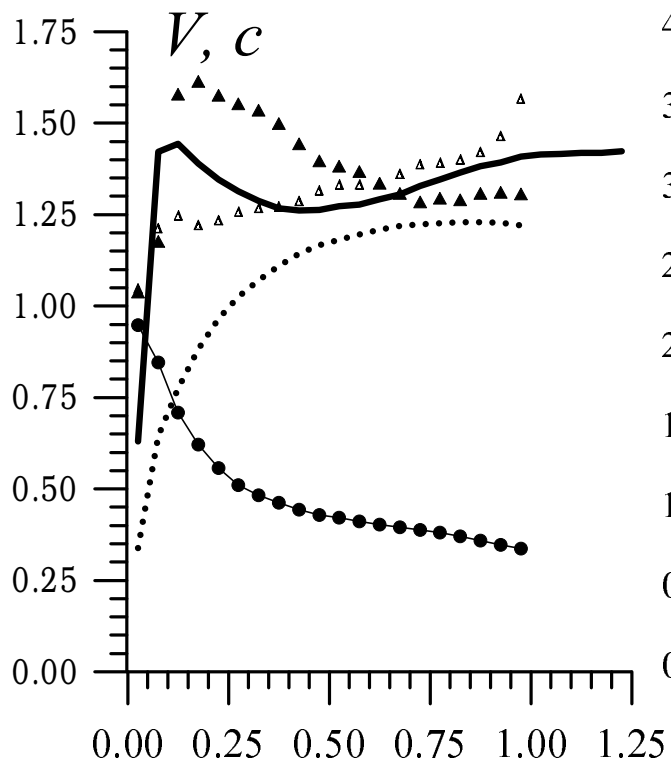


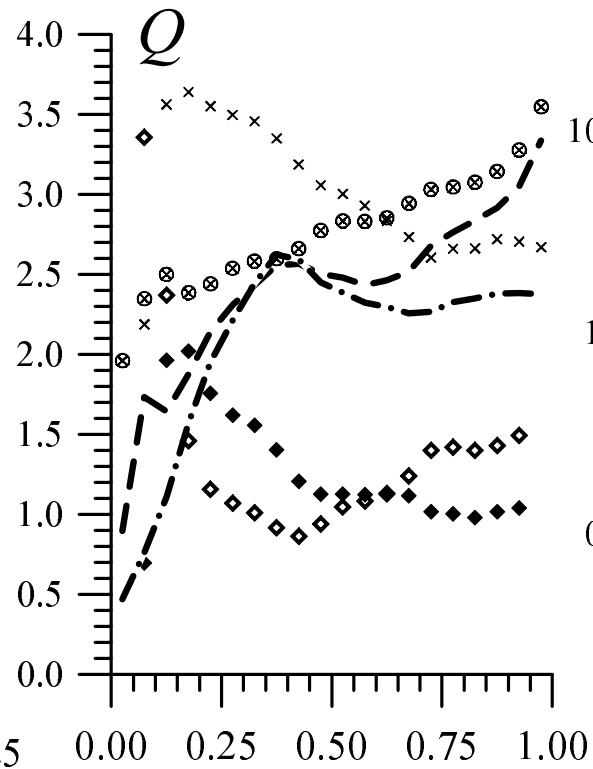
Fig.5(cont.)(c) Radial distributions of the ratio c_r/c_{crit} of the radial-velocity dispersions in the numerical models (curve 3 in Fig. 5a) to the critical values computed using the circular rotational velocity $V_c(r)$ (curve 1 in Fig. 5a) for 12 the Polyachenko–Polyachenko–Strel’nikov criterion (6) and 13 the Morozov criterion (5). Also shown are 14 $c_r/(c_T 2\Omega/\alpha)$ derived using the simplified criterion (4); 15 c_r normalized to $c^{(P)}Q_T^{(1)}$, which is a generalization of criterion (6) for the case of a finite-thickness disk, derived using (2); and 16 the ratio obtained for the Morozov criterion (5) in the case of an infinitely thin disk ($D = 1$). (d) Same as Fig. 5c using the disk rotational velocity $V(r)$ (see curve 2 in Fig. 5a).

Fig.5(cont.) (e) The Toomre parameter $Q_T(r)$ at the stability limit for a series of bulgeless models with various halo parameters. The bold thick curve is computed using (19).

Fig. 6 a)



b)



c)

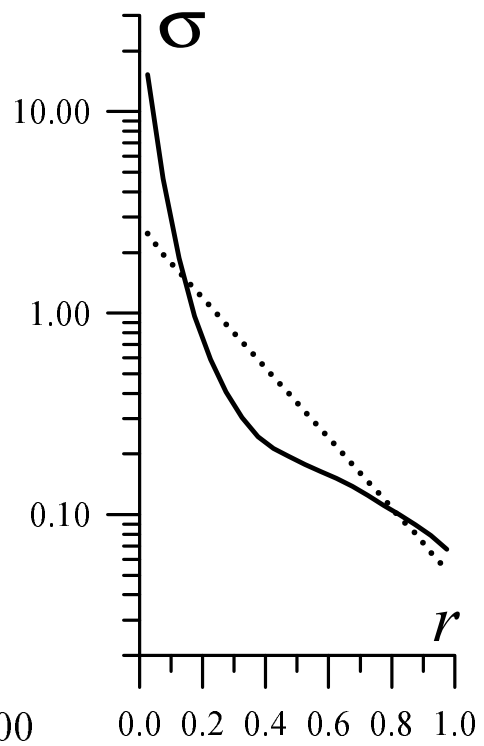
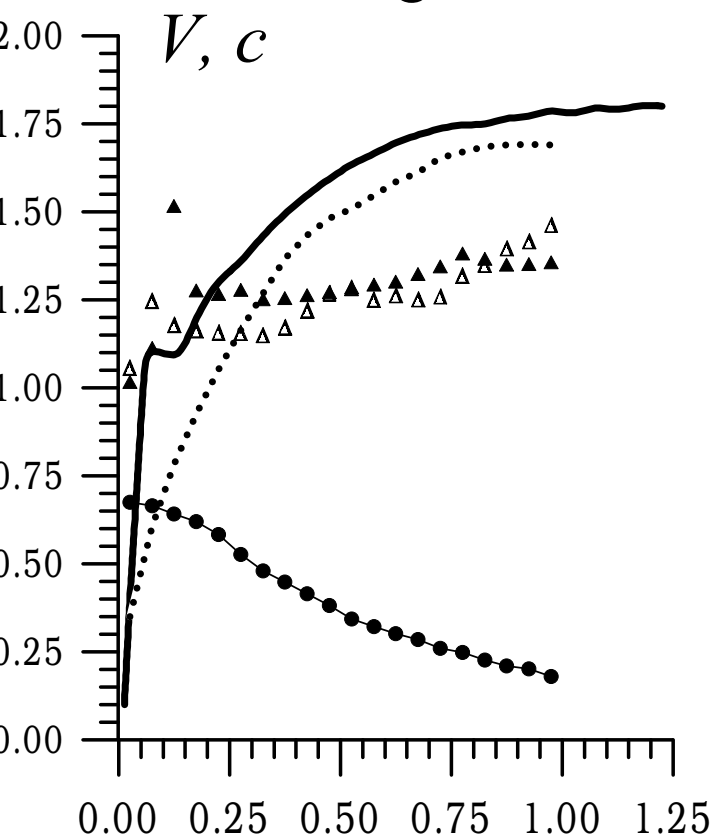
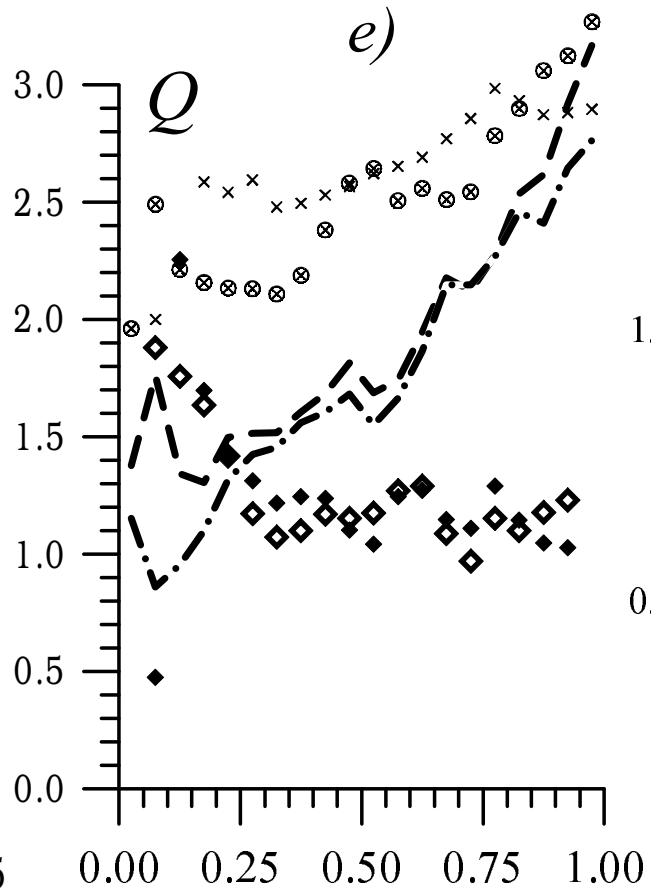


Fig.6. Bulgeless models that develop bars in the course of their evolution. (a)–(c) $M_h = 0.7M_d$, and $a = 2L$; (d)–(f) $M_h = 2M_d$ and $a = 1.6L$. Same notation as in Fig. 5. Plots c and f show azimuthally averaged surface-density profiles at the initial time (dashed) and after the development of a quasi-stationary state with a bar at $t \geq 25$ (solid).

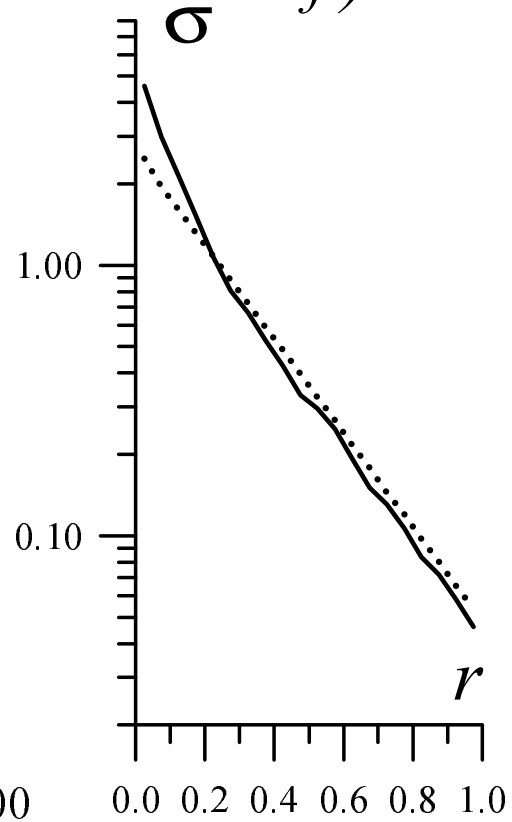
Fig. 6 *d)*



e)



f)



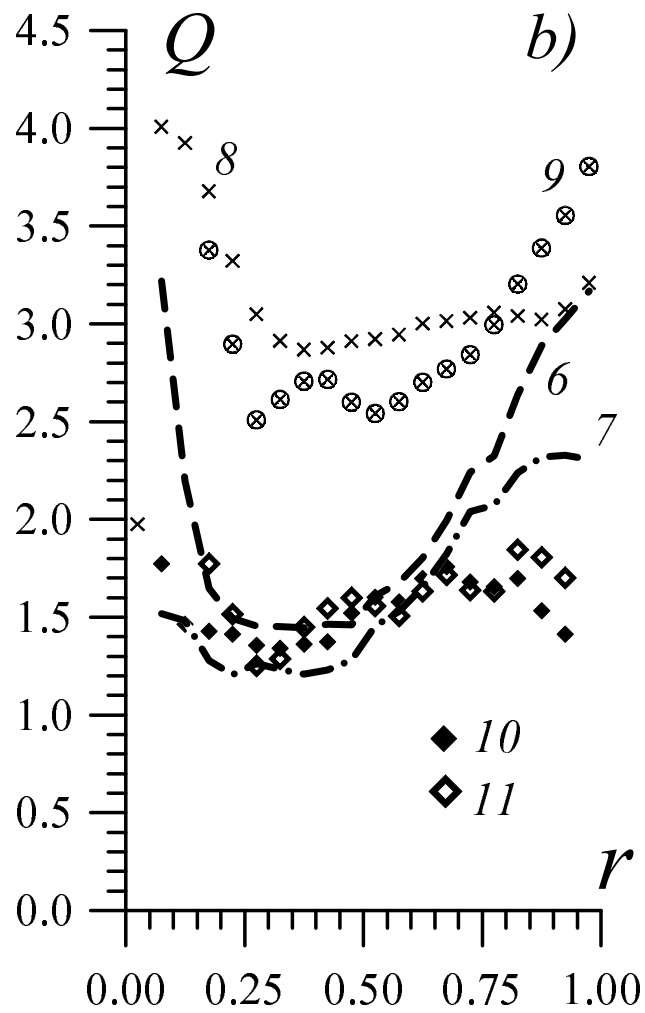
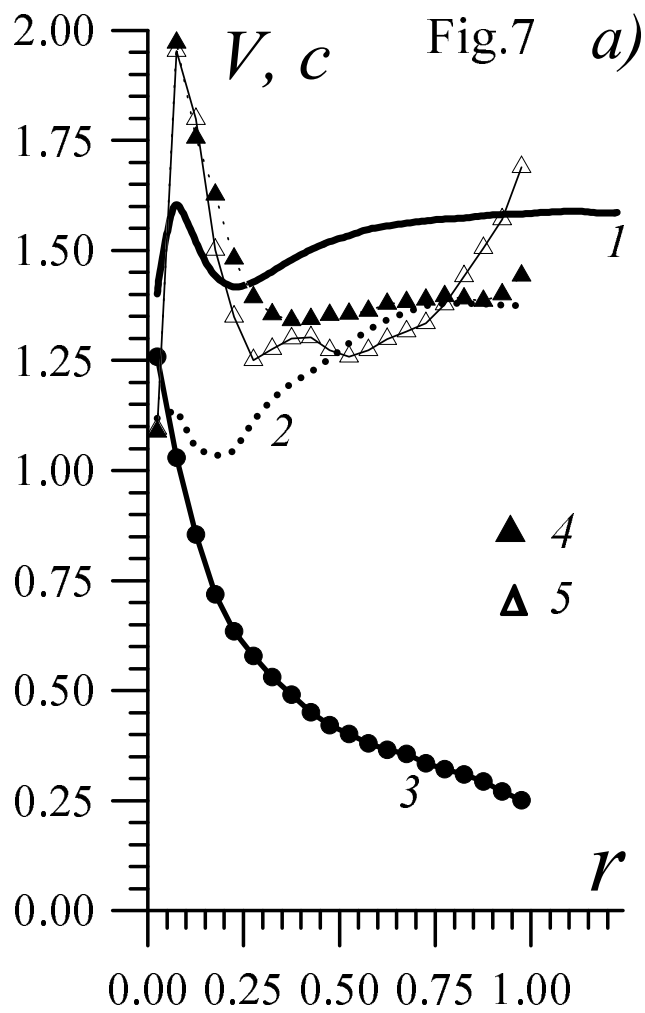


Figure 7. Disk parameters at the stability limit for models with bulges. (a)–(e) Radial dependences of the disk parameters (same notation as in Fig. 5). The mass of the halo within $r \leq 1 = 4L$ is equal to that of the disk, and the halo scale length is $a = 3.6L$. The bulge parameters are $M_b = 0.24M_d$, $b = 0.04L$, and $(r_b)_{max} = 0.5L$. (f) Toomre parameter $Q_T(r)$ computed using $V_c(r)$ at the stability limit for the series of models with bulges. The bold solid curve is based on (19). (g) Edge-on view of the disk at the end of the computation of the model shown in a. The dots show the positions of the particles. The model develops an appreciable bulge-like feature in the central region of the disk.

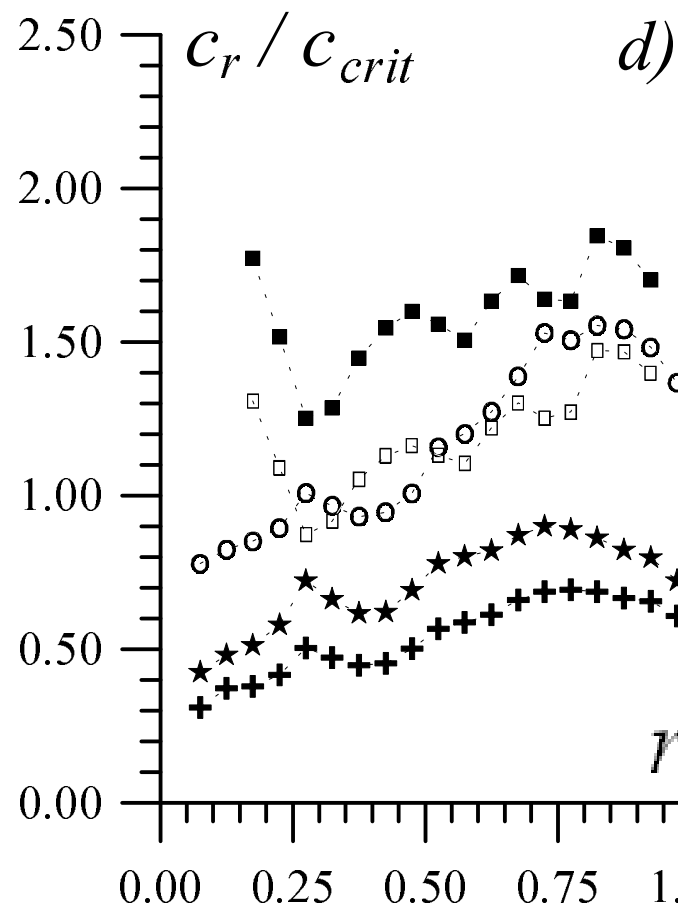
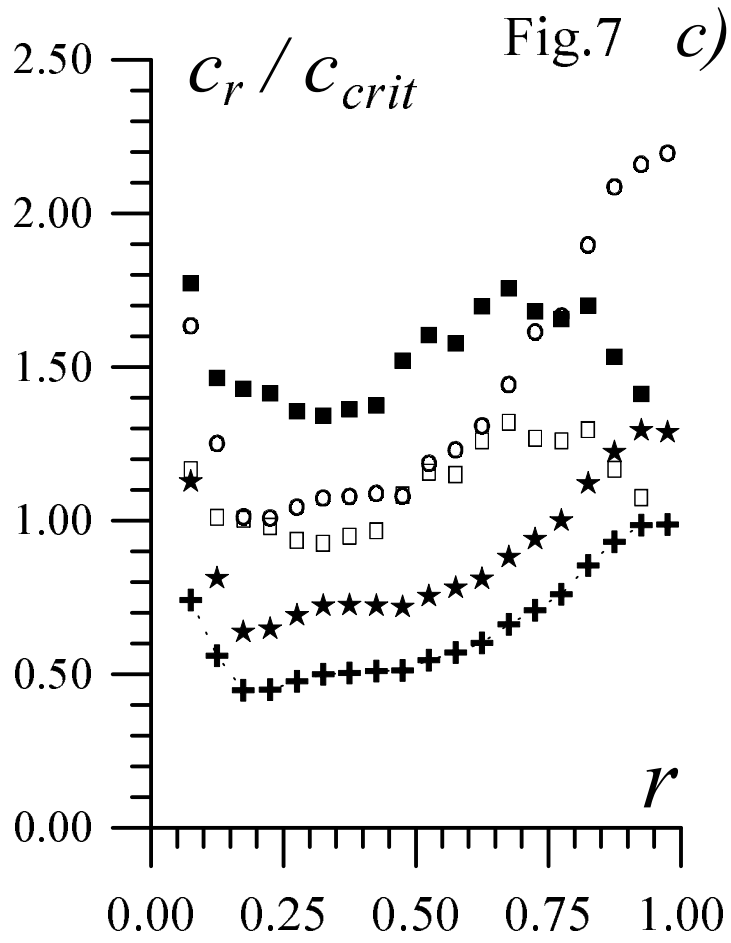
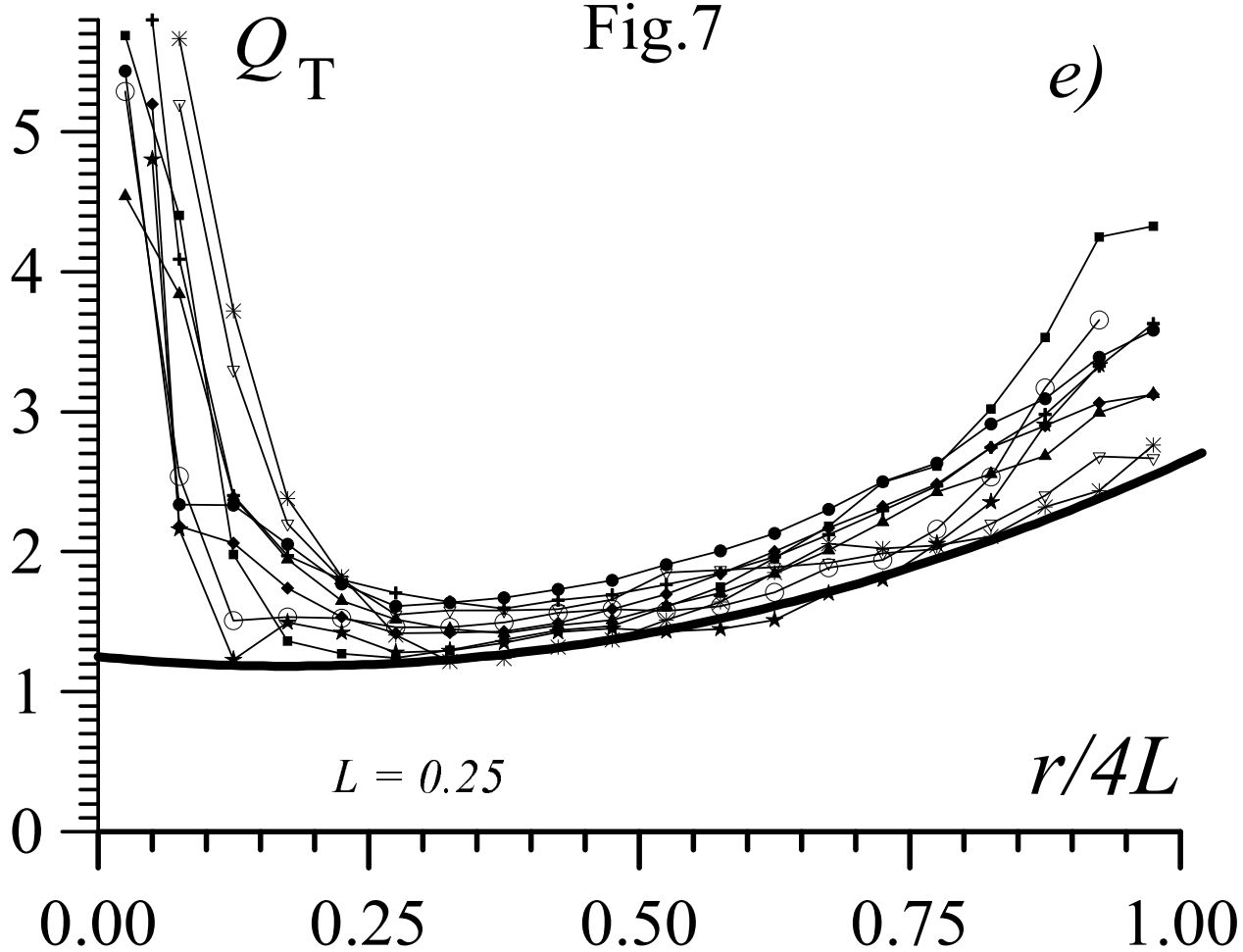


Fig.7

e)



$t = 46$

f)



Fig. 8

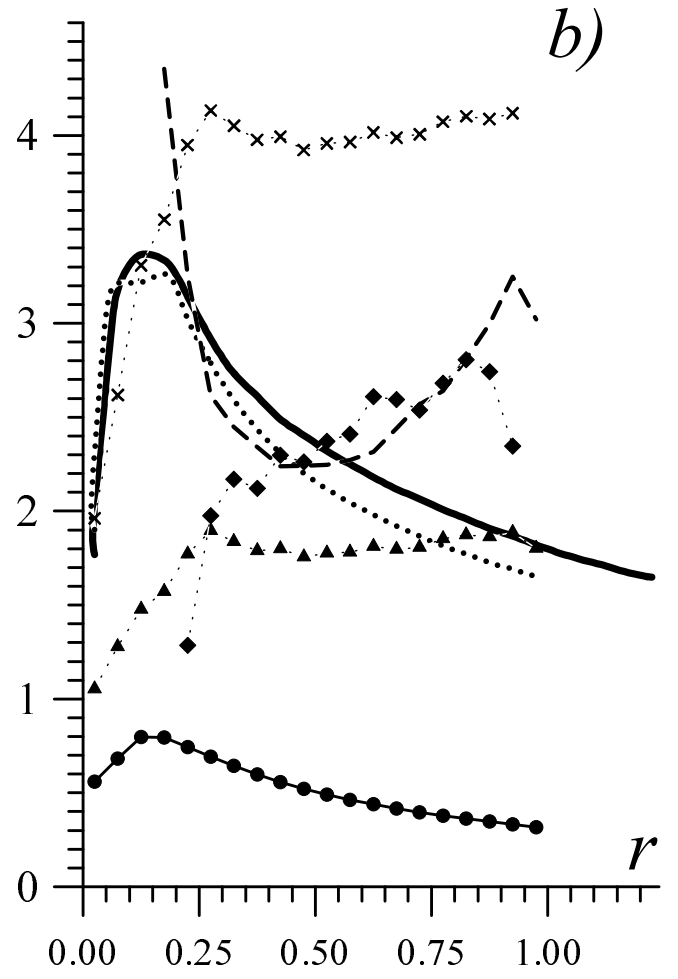
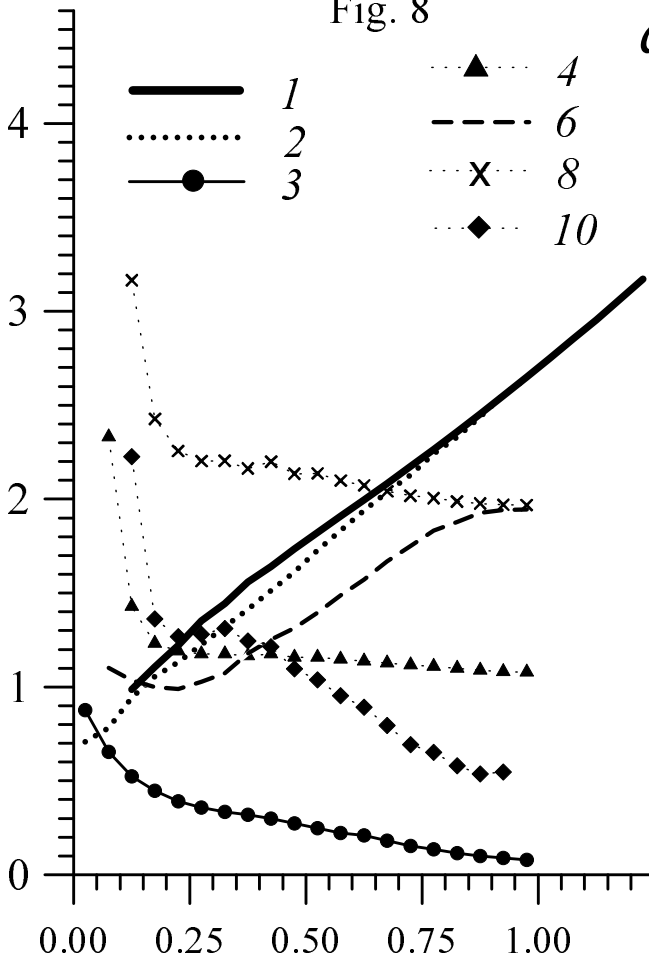


Fig.8 Radial dependences of the disk parameters in the adopted units for the cases when (a) a significant part of the disk rotates in accordance with a quasi-rigid law, and (b) the rotation at $r > L = 0.25$ is close to Keplerian: 1 the circular velocity $V_c(r)$; 2 the rotational velocity of the disk (stars) $V(r)$; 3 the radial-velocity dispersion $c_r(r)$; 4 the parameter S computed using (3) for the circular velocity; 6 the Toomre parameter Q_T computed using the circular velocity; 8 the critical Toomre parameter $Q_T^{(P)}$ computed using (6) with $V_c(r)$; 10 the critical Toomre parameter $Q_T^{(M)}$ computed using (5) with $V_c(r)$. The notation is analogous to that in Fig. 5.